IMPACT OF NANOPARTICLE SHAPE ON VES PERFORMANCE FOR HIGH TEMPERATURE APPLICATIONS

A Thesis

by

FAISAL TAMMAM NAJEM

Submitted to the Office of Graduate and Professional Studies of
Texas A&M University
in partial fulfillment of the requirements for the degree of

MASTER OF SCIENCE

Chair of Committee,	Hisham Nasr-El-Din
Committee Members,	Mahmoud El-Halwagi
	Jerome Schubert
Head of Department,	Jeff Spath

December 2018

Major Subject: Petroleum Engineering

ABSTRACT

Viscoelastic surfactants were introduced in hydraulic fracturing fluids as a proppant carrier in order to replace polymers which possess high potential for formation damage. Yet, VES technology is limited by its low thermal stability and high leak-off behavior in high permeability formations. This work aims to design a VES based hydraulic fracturing fluid assisted by various nanoparticles to enhance its rheological properties and extend its thermal stability to 285^{o}F and 350^{o}F.

This study examined iron oxide nanoparticles and nanorods and silica nanoparticles and nanorods with cationic and anionic VES solutions. A brine of 23 wt% $CaCl_2$ was used as a base fluid with different concentrations of both VES and nanoparticles. The dispersion of nanoparticles and rods was conducted by ultra-sonication for 10 minutes before the addition of VES. The rheology of each fracture fluid was assessed at 280 and 350^{o}F at a shear rate of 100 s^{-1}. Furthermore, both of the storage and loss moduli were examined to assess the fluid network structure and its carrying capacity for proppant delivery. The colloidal and macro properties of the nanoparticles and the VES mixtures were examined using a polarizing microscope before and after exposure to the high temperatures.

The addition of 7 pptg nanoparticles to the different VES solutions showed an extension and enhancement in the system rheological properties at high temperatures. The iron oxide nanoparticles extended the thermal stability of the fracturing fluid maintaining its viscosity above 75 cP for two hours compared to 30 minutes before its addition.

Although the microscopy examination showed homogenous distribution of the nanoparticles in the VES system before being heated, it showed agglomeration after the test which explained the failure after 2 hours. On the other hand, the silica nanoparticles succeeded to hold the viscosity above 75 cP for a longer time not showing degradation or loss in performance. This time the optical microscopy showed similar images before and after the test showing higher stability at 280^{o}F and absence of agglomerates.

This work examined the impact of two nanoparticles and nanorods on the rheological and thermal stability of cationic and anionic VES solutions. The optical microscopy study showed an ability to predict rheological properties of the fluid from its colloidal nature. The results from this work lay out a better design path for VES based fluids in fracturing and matrix acidizing technologies.

DEDICATION

To my father, mother, sisters, and brothers.

ACKNOWLEDGEMENTS

I would like to thank Dr. Hisham Nasr-El-Din for his support, guidance, and selflessness towards achieving my goals in pursuing my master in science in petroleum engineering and thesis. Through his extensive experience in the oil and gas industry, and his constant guidance and funding over my research, I learned a great deal, and would not have made it without him.

I would also like to thank my committee members, Dr. Mahmoud El-Halwagi, and Dr. Jerome Schubert, for their guidance throughout my research.

I to also acknowledge the Ministry of Higher Education of Kuwait, who funded my education throughout my undergraduate and graduate studies.

I want to also acknowledge Jim Crews, whose helpful discussion helped facilitate this research.

I have to thank all of my friends and colleagues at Texas A&M University because of their support and assistance, and making my time at Texas A&M a great and memorable experience.

Finally, I would like to thank my father, mother, aunt, and my sisters and brothers who have always supported me and encouraged me to keep being persistent in pursuing my degree. I am forever indebted to them.

CONTRIBUTORS AND FUNDING SOURCES

This work was supported by a dissertation committee consisting of Professor Hisham Nasre-El-Din and Professor Jerome Schubert of the Department of Petroleum Engineering and Professor Mahmoud El-Halwagi of the Department of Chemical Engineering.

Graduate study was supported by a fellowship from Texas A&M University and a dissertation research fellowship from Harold Vance Department of Petroleum Engineering.

NOMENCLATURE

CMC	Critical Micelle Concentration
wt%	weight percent
vol%	volume percent
VES	Viscoelastic surfactants
ISA	Ion strengthening agent
WLM	wormlike micelle
ppg	pounds per gallon
pptg	pounds per thousand gallon
cP	centipoise
nm	nanometer
s	seconds
s^{-1}	inverse seconds
SFC	semi flexible chain
min	minute
md	millidarcy
MPG	monoproylene glycol
q	scattering vector
SQW	square well potential
DLS	dynamic light scattering
TEM	Transmission electron microscopy

SEM	scanning electron microscopy
CT	computed tomagraphy

TABLE OF CONTENTS

Page

LIST OF FIGURES

Page

LIST OF TABLES

Page

CHAPTER I

INTRODUCTION AND LITERATURE REVIEW

1.1 Viscoelastic Surfactants

Shale fracturing is essential for shale hydrocarbon production. This process is critical due to the extremely low permeability of shale formations and their sensitivity to any kind of formation damage. Designing a successful fracturing fluid has to ensure minimal formation damage to the rock surface (Samuel et al. 2000).

Hydraulic-fracturing fluids pumped at large quantities are used to break down subterranean formation where hydrocarbons are trapped in. Pad fluids are first pumped in to cause the fractures and then additional fracturing fluids containing proppants are pumped in to keep the fractures open (Ghaithan et al., 2017).

Past field cases have shown that polymer based fracturing fluids have proven to be successful in producing fractures from a rock mechanics point of view. The usage of polymers have always been recommended for high temperature applications (Samuel et al. 2000). For decades, high molecular weight polymers that are cross-linked have been used to stimulate oil and gas wells. Polymers are used due to their high thermal stability, high viscosity, fluid leak-off controllability, and proppant transportability. Despite these properties, these polymers can leave residue in the formation and significantly decrease the fracture conductivity and formation permeability (Crews et al., 2008).

To solve this problem, thousands of wells have been pumped with viscoelastic surfactants (VES) in recent years. The surfactants are small molecules and are able to be pumped back completely without causing formation damage. They also have the advantage of being utilized with fewer additives compared to its polymer counterpart and are dissolvable in hydrocarbons during flow-back (Yang 2002).

Viscoelastic surfactants come in many forms and can be cationic, anionic, amphoteric, and nonionic. Cationic VES have been successfully used as fracturing fluids in many oilfields (Chase et al., 1997). VES are composed of a hydrophobic hydrocarbon tail, and hydrophilic ionic head. In aqueous solutions, the surfactant molecules agglomerate in a way that forms a hydrophobic inner layer and a hydrophilic outer layer, which are known to be micelles. Micelles can form in different shapes such as spheres, disks, and cylinders (Samuel et al., 1999). At low concentrations, the surfactants agglomerate and form spherical micelles. Wormlike cylindrical micelles start to form as surfactant concentration increases, with the addition of salt, and addition of acid (Crews and Gomaa 2012).

The controlling variables of the thermal stability and enhanced rheological performance of VES arise from the structure and functional groups they contain. Most VES contain a peptide bond between the hydrophilic head and hydrophobic tale. This bond is the most suitable for thermal cracking at higher temperatures due to acid hydrolysis at a temperature of 190^{o}F (Yu et al. 2012).When the VES undergoes hydrolysis, free fatty acids become produced. The bond breaking alters the ratio of the free fatty acids to the VES, which therefore controls the rheological performance of the VES when they form micelles. It has been found that a 3:1 ratio of fatty acids to VES was the optimum value for amido carboxybetaine surfactants.

The two main properties that VES display are viscosity and elasticity. There are two main mechanisms that help arise these properties, the first being when micelle-micelle entanglement occurs. The second is when additives such as nanoparticles form junctions with micelles and further interconnect with other particle-micelle junctions (Gurluk et al., 2013).

Despite the solutions that VES provides that address the problems caused by polymers, there are limitations. VES based solutions are very expensive and have a fracture-packing temperature limit of 200^{o}F. They also have the tendency to leak off into the formation due to their low molecular weight (Crews et al., 2008). Because of this poor fluid efficiency, more volume of fluid is required per treatment, and after leak off occurs, the residual fluid must be removed after the fracturing treatment (Huang et al., 2008).

1.2 Viscoelastic Surfactants and Nanoparticles

To address the VES limitations so much research has been done on the utilization of nanoparticles. Crews and Huang (2008) utilized 35 nm polyelectric nanoparticles as pseudo-crosslinkers to produce a network of micelle-micelle entanglement. This system had better proppant suspension and transportability compared to a typical borate crosslinked polymer fluids, and increased the viscosity by tenfold.

Pyroelectric and piezoelectric nanoparticles are extremely good at enhancing VES viscosity because they are small and stay well dispersed within the VES fluid when flowing into the target zone. Pyroelectric nanoparticles such as ZnO have their surface charge generated by heating and pressing, and these charges enhances nanoparticle-micelle behavior that increases solution viscosity (Crews and Huang, 2011).

Gurluk et al., (2013) proposed the use of magnesium oxide and zinc oxide nanoparticles to pseudo-crosslink VES micelles. With the addition of 6 pptg of MgO nanoparticles, the VES system was able to maintain a viscosity of 100 cp at 275^{o}F. Furthermore, the MgO nanoparticles appeared to have performed better than the ZnO nanoparticles. The MgO particle-surfactant interaction produced a more complex network

of micelles, which resulted in a higher viscosity (Gurluk et al., 2013). When conducting the oscillatory tests to determine elasticity measurements of the fluid, it was found that the dominant factor at room temperature was the storage modulus, and at high temperature it was the loss modulus. At a certain critical frequency, response of the particle dispersion changes the fluid behavior from being viscous to elastic. The moduli data of the 4 vol% VES samples showed that they were strongly frequency dependent. The storage modulus G' of the VES fluid displays the energy storage and can be related to the complex crosslinked networks. The storage modulus decreased which in turn means that the network structure weakened due to the formation of spherical micelle aggregates around the surface of the particles. This caused the viscous forces to dissipate and most of the energy stored was considered negligible.

MgO and ZnO nanoparticles can be added to the VES system before being pumped downhole (Huang and Crews, 2008B). However, for MgO, if present in powder form, they cannot be dispersed in water because an outer layer of $Mg(OH)_2$ will form. In this case, the continuous phase can be propylene glycol; it is miscible in water and generates a microemulsion that can suspend the nanoparticles very well (Huang and Crews, 2008C).

Li et al., (2018) introduced the concept of fracturing with hydrocarbon based fluid called gelled oil fluids. They typically contain crude oil, condensate, diesel, or mineral oil. They are used instead of water based fracturing fluids to eliminate the need of for most fluid additives such as biocides, clay stabilizers, and corrosion inhibitors. Low molecular weight oil gelling agents such as alkyl phosphate esters are used to avoid formation

damage, and nanostructured clay additives are used to enhance the viscosity of these fluids. Adding many different types of nanoclays was found to have significantly increased the viscosity of the gelled oil fluids (Li et al., 2018).

Ozden et al., (2017) tested two different nanomaterials on VES and were able to withhold a viscosity greater than 100 cP. Even when tested at 350^{o}F, the VES system was able to maintain a viscosity of greater than 100 cP for 140 minutes. In this study, a solution containing 5 vol% VES and 30wt% $CaCl_2$ brine was utilized. After adding the VES to the brine, two nanomaterials were tested and compared with each other and a base fluid to assess their rheological performance with heating from room temperature gradually to 350^{o}F under 400 psi. The shear rate was kept constant at 100 s^{-1}. Both nanomaterials were kept confidential and identified as nanomaterial-I and II.

For the solutions containing nanomaterial-I, 2 solutions were prepared; one containing 6 pptg and the other containing 12 pptg of the same material. Their viscosities were measured and both displayed higher viscosity above 200^{o}F. When taking the average of the viscosities at 250^{o}F and 350^{o}F, the viscosity enhancement relative to the base fluid was about 20% for the 6 pptg fluid, and 24% for the 12 pptg fluid. For the other set of tests involving nanomaterial-II, a similar base fluid was prepared using 5 vol% VES and 30wt% $CaCl_2$. This time the two concentrations of nanomaterial-II being compared with each other were 2 and 4 pptg. After the rheology tests, it was observed that both of these nanomaterials displayed higher viscosity above 230^{o}F. When taking the average the viscosities again at 250 and 350^{o}F, the viscosity enhancement compared to the base fluid was 15% and 23% for the 2 pptg and 4 pptg solutions, respectively. The rheology tests

showed that both nanomaterials caused stronger interactions between the VES micelles and them, which caused the viscosities to be enhanced.

The long-term stability of the VES fluids was also tested at 350^{o}F. The viscosity of solutions containing both of these nanomaterials were compared to each other and their respective base fluids at the same exact concentrations and conditions of the previous tests. The viscosity of the base fluid was 89 cP at 200 minutes at 350^{o}F. At the same temperature, the solution containing 6 pptg of nanoamaterial-I displayed a viscosity of 110 cP and presented an enhancement of 24%. The viscosity of the fluid containing 12 pptg of nanomaterial-I remained above 110 cP for 180 minutes and then declined to 104 cP and maintained this viscosity. The viscosity improvement was reported to be 17% of compared to the base fluid. For nanomaterial-II, the VES solutions containing them at 2 pptg and 4 pptg also improved the long-term stability compared to the base fluid at 350^{o}F. The viscosity maintained above 110 cP for over two hours.

Oscillatory tests were further conducted to characterize the storage and loss modulus corresponding to the solid-like and fluid-like contributions to the stress response of the VES based fluids. The measured storage and loss modulus as a function of frequency at 350^{o}F were measured for the base fluid, and both types of nanoparticle-enhanced fluids. The behaviors were similar to those of other viscoelastic fluids; the loss modulus dominated and the fluids behaved more viscously at lower frequencies. At higher frequencies, the storage modulus dominated and the fluids behaved more elastically. For the base fluid, the loss modulus was higher than the storage modulus up until a frequency of 3.5 Hz is achieved. This frequency is the crossover frequency and is typical for VES

(Fakoya and Shah 2013), and beyond it, the loss modulus begins to decrease and the storage modulus continues to increase as the frequency increases. With the addition of both nanomaterials I and II, the VES fluids displayed higher values of storage and loss moduli.

The moduli of all the VES fluids including the base were also measured as a function of temperature holding a constant frequency of 4 Hz. The storage modulus of the base fluid increased with increasing temperature up to 300^{o}F and then started to decrease. When adding nanomaterial I and II, the storage modulus was enhanced at temperatures above 200^{o}F. This indicates that the addition of these nanomaterials may have resulted in increased interconnected and aggregated micellar networks.

Further work has been done with VES and nanoparticles except with the utilization of seawater instead of fresh water. Sangaru et al., 2017, prepared fracturing fluid using local seawater from the Arabian Gulf, and filtered it to remove any suspended solids. An ionic strengthening agent (ISA) was also added to the seawater at 30wt%, and centrifugation was conducted to remove further suspended solids. To the seawater brine, VES was then added at 9.5 vol% and this served as the base fluid. Two different types of nanoparticles were added separately to formulate two more fracturing fluids. Both nanoparticles' size were at an average of 40 nm and both were added at the same concentration to the VES at 24 pptg. The rheology of the base fluid was tested with a temperature ramp from 90^{o}F to 375^{o}F at constant shear rate of 100 s^{-1}. After this temperature profile was established, the rheology tests of the base fluid and the

nanoparticle-enhanced fluids were conducted at different shear rates from 0.01 s^{-1} to 600 s^{-1} at different intervals.

The results of the rheology tests showed that peak viscosity of the base fluid was achieved at 237^{o}F and another minor stable viscosity was observed from 305 to 313^{o}F. After this range the viscosity rapidly declines. From these data points, five different temperatures from 180 to 300^{o}F were selected at 30^{o}F intervals, and the viscosity was evaluated at varying shear rates for the three fluids. It was observed that all the fluids had similar shear thinning behavior at all temperatures. This behavior is usually observed above a critical shear rate, and this shear rate signifies the relaxation time for the fluid, of which beyond the applied stress on the fluid, structural rearrangement occurs in the entangled cylindrical micelles. It is this event that results to the decrease of the viscosity as the shear rate continues to increase. With the fluids in this study, the lack of a viscosity plateau signifies that the fluid consists of a dense wormlike micellar network leading to the formation of viscoelastic gel (Zhang et al., 2015). At temperatures of 180, 210, and 240^{o}F, all three solutions have similar viscosities with respect to the shear rate range. This indicated that the addition of the nanoparticles does not have any significant impact on the viscosity enhancement of the fluids. At higher temperatures, 270 and 300^{o}F, significant differences and enhancement were observed. The VES solution containing nanoparticle-1 achieved a viscosity around 8.7 times higher than that of the base fluid. Similarly, the VES containing nanoparticle-2 displayed 3.5 times higher viscosity than that of the base fluid at 300^{o}F.

At 270 and 300^{o}F, differences were observed in the shear stress-shear rate plots. A shear tress plateau was observed with the fluids that contained both nanoparticles. The shear stress value at 0.01 s^{-1} can be considered as the apparent yield stress for all the fluids, and at 270^{o}F, there was a 4.9 and 2.9 times increase of this value for nanoparticle-1 and 2, respectively. At 300^{o}F, there was an 8.7 times increase and a 3.5 times increase in the yield stress values, for the VES fluids enhances by nanoparticle-1 and 2, respectively. These value increases in the apparent yield stress values can be interpreted as better proppant carrying capacities for the fluids (Crews and Huang 2008).

At lower temperatures from 180 to 240^{o}F, the viscosity of the fluid is in the phase where it increases with increasing temperature. The increase in temperature disfavors the intermolecular hydrogen bonding which induces dehydration of the polar head groups of the micelles. This leads the head group to decrease in cross sectional area, which leads to formation of elongated wormlike micelles. The elongated micelles then tangle which causes higher viscosity (Feng, Chu, & Dreiss, 2015). This mechanism suggests that the nanoparticles do not have an impact on the VES yet, but as the temperature increases, greater degree of hydration causes branching in the micelles, which leads to a decrease in their length. When the branching occurs, the nanoparticles then act as pseudo-crosslinkers that crosslink between the micelles, which offsets the loss of viscosity. Since the micelles are already elongated and tangled at lower temperatures, no crosslinking occurs when the nanoparticles are present until the temperature increases.

Zeta potential analysis was also conducted in this study to understand why nanoparticle-1 enhanced the low shear viscosity of the VES compared to nanoparticle-2.

Nanoparticles-1 and 2 were separately suspended in deionized water and their average zeta potential values were +23.7 and 18 mV, respectively. Nanoparticle-1 displayed a broader zeta potential distribution extending up to 45 mV and nanoparticle-2 only reached 30 mV. The higher the zeta potential value, the more likely the particle can pseudo crosslink between the micelles because stronger electrostatic interactions are present as compared to nanoparticle-2.

The use of silica nanoparticles has also been investigated by Nettesheim et al., (2008). 30-nm silica nanoparticles were added to threadlike micellar fluid at low concentrations and the system displayed an increase in low shear rate viscosity, elastic modulus, and relaxation time.

Sangaru et al., 2016, further tested 2 different confidential nanoparticles with VES. The concentration of the VES was 9 vol% and was mixed with seawater from the Arabian gulf. 30 wt% ISA was dissolved in the solution and 24 pptg of each type of nanoparticles was added to formulate the fracturing fluids. The forth fluid however was a mixture of both types of nanoparticles in 1:1 ratio. All the nanoparticles were dispersed in 5 ml of deionized water and then added and mixed to the VES solution. Fluid loss was measured over 70 minutes by measuring the weight of the fluid released from the pressurized container. The API fluid loss value was measured by 2.V30, where V30 is the volume of the fluid loss at 30 min. The base fluid loss was complete and measured by $2xVx(30/t)^{1/2}$, where V_t is the volume at time t when the blow-through occurs.

1.3 Brine Compatibility with VES Solutions

The Hoffmeister series can be viewed to predict the interaction between different brines and the VES micelle-nanoparticle junctions. It ranks the relative influence on different ions on the physical behavior of colloidal systems. The smaller the cation, the larger the charge density (Zhang et al., 2006).

$$Cs^+ > Rb^+ > K^+ > Na^+ > Li^+$$

$$CNS^- > I^- > Br^- > Cl^- > F^- > NO_3^- > ClO_4^-$$

Fig. 1- Hoffmeister series.

It was observed by Gurluk et al. (2013), that adding KCl and NaCl to amidoamine oxide surfactant containing 6 pptg 30 nm MgO nanoparticles enhances the viscosity and extends the time of viscosity stability at 200°F. However, the interaction of micelle-nanoparticle and divalent salts is much stronger than monovalent salts. Divalent salts such as $CaCl_2$ and $CaBr_2$ enhance the viscosity much more than monovalent salts at higher temperatures. In this study apparent fluid viscosity was measured using 4 vol% VES in brine containing 7 wt% KCl at 200°F and at a shear rate of 10 s^{-1}. The MgO nanoparticles were added to the VES fluid via a slurry in monopropylene glycol (MPG) at a ratio of 2.5 ml MPG to 1 gram of nanoparticles. The same rheological tests were conducted on a 4 vol% VES solution, this time containing 20 wt% NaCl and at temperatures of 200 and 275°F. The MPG was added in small quantities and thus has negligible effect on the VES micelle length. They were removed by the addition of brine water upon mixing. A shear

rate sweep was performed from a range of 100 to 1 s^{-1} for the 7 wt% KCl solution at a temperature range of 100 to 200^{o}F. The sample was heated to 100^{o}F at first and sheared at 100 s^{-1} for 30 minutes, then the shear rate sweep was run. The same procedure was followed but for temperatures of 150 and 200^{o}F. This procedure was also repeated with the 20 wt% NaCl solution with and without nanoparticles.

The results in this study indicated that for the 4 vol% VES in 7 wt% KCl brine, the addition of nanoparticles stabilizes the viscosity at 200^{o}F, while without nanoparticles the viscosity decrease after a while. It also showed that the VES in KCl solution has a much better interaction with the MgO nanoparticles than the ZnO nanoparticles. As for the VES solution containing 20wt% NaCl, at 275^{o}F and with the shear rate kept at 10 s^{-1}, the best result is achieved upon addition of MgO nanoparticles. Adding ZnO nanoparticles to the solution only leads to the viscosity decreasing rapidly. However when the temperature is decreased to 200^{o}F for the same solution, the apparent viscosity is actually enhanced and gives higher viscosity than that of the solutions containing the MgO nanoparticles or none at all. This phenomena may indicate that the surface forces generated by each type nanoparticle vary with temperature. Temperature does also play a role in wormlike micelle end stability which therefor plays a role in the length of the micelles. When the temperature of the VES reached to approximately 150^{o}F, then end cap tends to grow, but when reaching temperatures beyond that, the endcap thermodynamic energy is not stable, and the micelle length decreases.

The low shear rate measurements were taken after each fluid containing 7 wt% KCl and 20 wt% NaCl brine were held static at 100, 150, and 200^{o}F. Adding the MgO

nanoparticles enhanced the viscosity of the VES. For the KCl solution, the interaction of the VES with MgO nanoparticles is much stronger than that of the VES and ZnO nanoparticles. However, with the 20 wt% NaCl solution, the ZnO nanoparticles causes a much significant viscosity increase than the MgO nanoparticles present or with none present at all.

Finally the last part of this study involved investigating the use of different concentrations of MgO nanoparticles with 4 vol% VES and 14.2 ppg $CaBr_2$, the only divalent salt tested. The results showed that varying the concentration of MgO from 2-10 pptg yielded the roughly the same viscosity. However, when decreasing the quantity of MgO nanoparticles to 0.5 pptg, the viscosity of the VES enhances greatly and is stabilized for at least 150 minutes.

Past studies have illustrated that the critical micelle concentration (CMC), the concentration at which micelles start to form after addition of VES, is reduced as the concentration of the counter ions increases. Addition of salts such as $CaCl_2$ and $CaBr_2$ at 10 to 23 wt% can have such an effect on the micellization of VES. The degree of micellization depends on Debye length, which is a function of the electrostatic interaction between the both chemical species in solution (Rehage and Hoffman 1991). As the concentration of the cation increases, more screening occurs of the charged head groups and repulsion between the surfactant heads which leads to easier and stronger pseudo crosslinking micellization (Zhang and Cremer 2006; Goodwin 2009). However, as the counter ion concentration increases, excessive screening of surfactant head groups occurs

which leads to further networking and branching, thus causing phase separation (Drye and Cates 1992).

1.4 Theory

Models such as the Cates model can be utilized to demonstrate the dynamics of wormlike micellar solutions (Drye and Cates 1992; Cates et al. 1990; Spenley et al. 1993). It considers two primary relaxation times related to the reptation of the micelles, λ_{rep}, and the micellar breakage λ_{br}. In the case where $\lambda_{br} \ll \lambda_{rep}$, which defines fast breakage, the single relaxation time can be defined as the geometric mean of λ_{rep} and λ_{br}:

$$\lambda_r = \sqrt{\lambda_{rep}\lambda_{br}}$$

The mean relaxation time, λ_r, defined as the point of crossover in the viscoelastic spectra. The frequency, ω, is defined as:

$$\omega = {\lambda_{br}}^{-1}$$

The frequency corresponds to the local G" which deines the plateau modulus G_P. The rubber elasticity relates the mesh size, ξ_M, directly to the network density, ν:

$$G_P' = \nu k_B T \propto \frac{k_B T}{\xi_M^3}$$

The loss modulus at the minimum, contour length $\bar{L}$, and the entanglement length l_e are all related by the following equation:

$$\frac{G_p'}{G_{min}''} \approx \frac{\bar{L}}{l_e}$$

The entanglement length is related to the mesh size and persistence length, l_p, by:

$$l_e \approx \frac{\xi_M^{5/3}}{l_p^{2/3}}$$

The persistence length can be measured by dynamic light scattering, flow birefringence, high frequency rheology, or neutron spin echo measurements (Farge et al. 1993; Zilman et al. 1996; von Berlepsch et al. 1998; Shikata et al. 1994; Willenbacher et al. 2007a.; Willenbacher and Oelschlaeger 2007; Nettesheim et al. 2007).

Scattering of WLMs in solution may be described by the form factor of a semiflexible chain (SFC) when accounting for excluded volume effects (Pedersen and Schurtenberger 1996). Depending on the magnitude of the scattering vector, q, micellar solutions will exhibit different behavior as the magnitude decreases. At high scattering vectors, the spectra displays oscillations, which in part is due to the cross-sectional dimension of the wormlike micelles. At intermediate scattering vectors, the intensity decreases to q^{-1}, which is typical of elongated linear objects such as WLMs. Finally, at lower scattering vectors, a transition occurs between systems when the intensity changes according to q, from $q^{-1.5}$ to q^{-2}. WLM network density fluctuations and interparticle correlations produce great divergence from simple SFC scattering at low q.

For solutions containing both WLMs and nanoparticles, scattering is a function of both components that are highly dependent and intertwined together in term their partial structure factors (Klein 2002; Kline and Kaler 2002). A model that can be applied to interparticle interactions is the idealized square well potential (SQW). The potential is defines as

$$U(r) = \begin{cases} \infty, & r < 0 \\ -\varepsilon, & 2R_{hs} \le r \le 2R_{hs}\lambda \\ 0 & r \ge 2R_{hs}\lambda \end{cases}$$

where R_{hs} is the hard sphere radius, ε is the depth of the potential with units of $k_B T$, and λ is the relative width where

$$\lambda = 1 + \frac{\Delta}{R_{hs}}$$

DLS is used to probe where the diffusivity of the nanoparticles within the WLM solution. Since both the nanoparticles and WLMs scatter light, two modes are observed in the field-correlation function measured (Nemoto et al. 1995). A model can be utilized to illustrate the diffusion of a sphere into a viscous fluid. The model can be expressed as

$$g_t(\tau) = A g_m(\tau) + (1 - A) g_p(\tau)$$

Where $g_m(\tau)$ is the field correlation function of the wormlike micellar solution containing no nanoparticles. This is acquired by measuring the intensity autocorrelation function by using the Siegert relation. $g_p(\tau)$ is the field correlation for a diffusing spherical particle, which is calculated using the Stokes-Einstein relation:

$$D_0 = \frac{k_B T}{6\pi\eta_s R_h}$$

$$g_p(\tau) = \mathrm{e}^{-\mathrm{D}\mathrm{q}^2\tau}$$

Since the hydrodynamic radius of the nanoparticles are measure independently, the apparent viscosity is the only adjustable parameter of bulk fluid, which makes this method effective in measuring the apparent viscosity of the fluid suspending the nanoparticles.

CHAPTER II

MATERIALS AND METHODOLOGY

2.1 Silica Nanorod Synthesis

The silica nanorods were not purchased thus they were synthesized in the lab by means of surfactant templating. The methodology of preparation of these nanorods was proposed by Rahmani et al. (2017). First, 100 mg of C_{18}TAB, 50 mL ultrapure water, and 5 mL ethanol were stirred at 323K for 20 min at 750 rpm in a 100 mL round bottomed flask. Then 575 µL TEOS and 350 uL NaOH were added to the solution. The mixture was kept stirring for 2 hours at 323K. After 2 hrs, the solution is cooled down while stirring to room temperature. It was then centrifuged for 15 min at 5200 g. The sample was then extracted twice with 6 g/L ammonium nitrate in ethanol to remove the surfactant, and underwent sonication for 30 min at 323K in each extraction. The rods were then washed three times with ethanol, water, and then ethanol, and were dried under vacuum for a few hours.

2.2 Iron Oxide Nanorod Synthesis

To prepare the iron nanorods, the co-precipitation method was utilized. Ferrous and ferric chloride were dispersed in water at 2:1 molar ratio and were then reacted with a NaOH solution of pH 12 while being sonicated. Sonication was used instead of conventional stirring to force the product to precipitate as rod-shaped. The NaOH was reacted with the ferrous/ferric chloride mixture dropwise through a glass burette, and the sonication was set at a strength of 49kHz for 4 seconds with a break of 2 seconds to avoid heating of the solution and deformation of the iron oxide nanorods. The solution was left for 1 hour to ensure complete reaction after all the ferrous/ferric solution was added to the NaOH. The

solution was then washed with deionized water and left to dry for 24 hours. This methodology was proposed by Hanafy et al. (2014).

2.3 VES Solution Preparation

To prepare the VES solutions, a simple three step method was implemented. First, 23 g calcium chloride was dissolved in deionized water. Then, 0.072 g of nanoparticles/nanorods were dispersed in the solution using ultrasonication for 15 minutes. Finally, 4 ml VES was mixed in the solution, and mixed using an impeller for 10 minutes.

2.4 Nanoparticles' and Nanorods' Impact on Rheology

The designed fracturing fluid was tested at VES concentrations of 2 and 4 wt% to determine the effects of varying concentrations on the system's additives, which was the brine, nanoparticles and nanorods. The brine used was $CaCl_2$ dissolved in water at 23 wt%. The nanoparticles and nanorods were added in at a concentration of 6 pptg. Each system was tested at 280^{o}F and then again at 350^{o}F at the same conditions. The shear rate was kept constant at 100 s^{-1} for one hour. All of these systems were compared to VES systems with no nanoparticles/nanorods at the 2 and 4 wt% VES and at the same operating conditions (280 and 350^{o}F).

2.5 Grace M5600 Rheometer

The rheometer used in this experiment was the Grace M5600 rheometer. The capacity size per sample is 32 to 78 ml. The temperature range it can be operated on ranges from 20^{o}F

to 500^{o}F. The viscosity range for the rheometer is 0.5 to 5000000 cp. Its shear rate range is from 0.00004 to 1870 s^{-1}.

2.6 Fluid Microscopic Assessment

Both the before and after rheology fracturing solutions were examined under an optical microscope at 5, 10, 20, and 50x to examine the nanoparticle dispersal in the VES solutions, VES separation, and microemulsions. The produced images was processed using Image-J to examine the differences between each solutions and the effects of the rheology tests on them.

2.7 ZetaPALS Zeta Potential Analyzer

The ZetaPALS zeta potential analyzer was used to measure the particle size distribution and surface charge of the micelles and nanoparticles. Dynamic light scattering was used to measure the particle size distribution. The changes of the micelle size was monitored before and after the addition of the nanoparticles and nanorods. Nanoparticles and rods dispersed in water, nanoparticles and $CaCl_2$, and nanoparticles and $CaCl_2$ and VES were evaluated to examine the surface charges on each species and the change in the overall charge of the solutions. Understanding the charge interactions between each individual component can help understand the adsorption process of the VES on the nanoparticles.

2.8 Proppant Settling Test

The proppant-carrying-capacity of the VES fluids were evaluated in a HPHT see-through-cell. The fracturing fluids containing no nanoparticles and containing silica nanospheres were preheated and stirred to suspend the proppants. The preheated fluid was then transferred to the see-through-cell, were the conditions of that cell were 400 psi and 280^{o}F. Photo images were taken periodically to determine the proppant settling rate during a 4 hour period.

2.9 Dynamic Oscillatory Measurement (DOM)

DOM is an established method to evaluate the microstructure of fracturing fluids. It does so by measuring the storage (G') and loss moduli (G"). These moduli represent the elastic and viscous behavior, respectively. This experiment involved 2 stages. The first stage involved a set of experiments that were conducted utilizing an amplitude sweep to determine the strain value at which the fracking fluid moves from linear to non-linear viscoelastic behavior. The second stage involved a frequency sweep once the critical strain value was determined. The frequency sweep was conducted between 0.1 to 0.4 rad/s.

2.10 Filter Loss and Formation Damage Analysis

To examine the impact of silica nanospheres on the fracturing fluid filtration loss and residual formation damage after VES injection, a coreflood setup was utilized. Buff Berea sandstone cores were used in the experiment to evaluate the fluid loss rate using a differential pressure of 400 psi at a temperature of 280^{o}F. The dimensions of the cores were 6 in. in length and 1.5 in. in diameter. To ensure linear flow along the core and avoid radial flow, an overburden pressure of 1000 psi was set. The cores were then scanned

using computed tomography. The pressure drop analysis was then correlated to the filtration rate to determine the extent of damage along the core. The VES based fracturing fluid and the fracturing fluid containing silica nanospheres were both examined. The composition of the fracturing fluid was 4 wt% VES, 23 wt% $CaCl_2$, and the silica nanospheres were added at 7 pptg. Core permeability was evaluated before and after the damage and the cores were subsequently soaked in mutual solvent overnight to examine the VES fluid breakability in the presence and absence of silica nanospheres. The final permeability of the clean core was measured and CT scanned to track the breakability of the VES after soaking it with mutual solvent.

CHAPTER III

EXPERIMENTAL RESULTS[i]

3.1 Silica Nanorods Analysis

The silica nanorods are relatively large compared to the ironoxide nanorods synthesized. They typically average to 500 nm in length and 286 nm in diameter and are uniformly shaped. There was large size distribution with some nanorods reaching roughly 2 microns in length. The XRD analysis displayed a broad singular peak and the data showed that the d spacing indicated that the particles are in the submicron size and a singular crystal system.

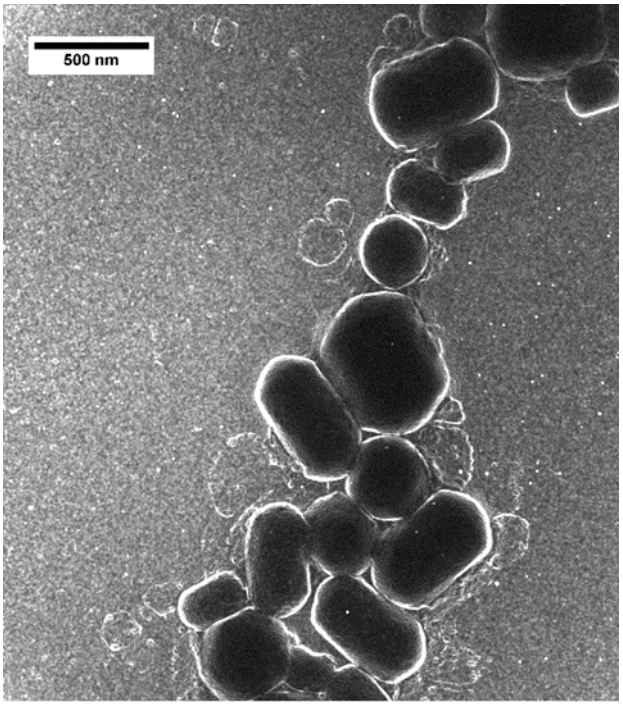

Fig. 2- TEM image of lab-prepared silica nanorods.

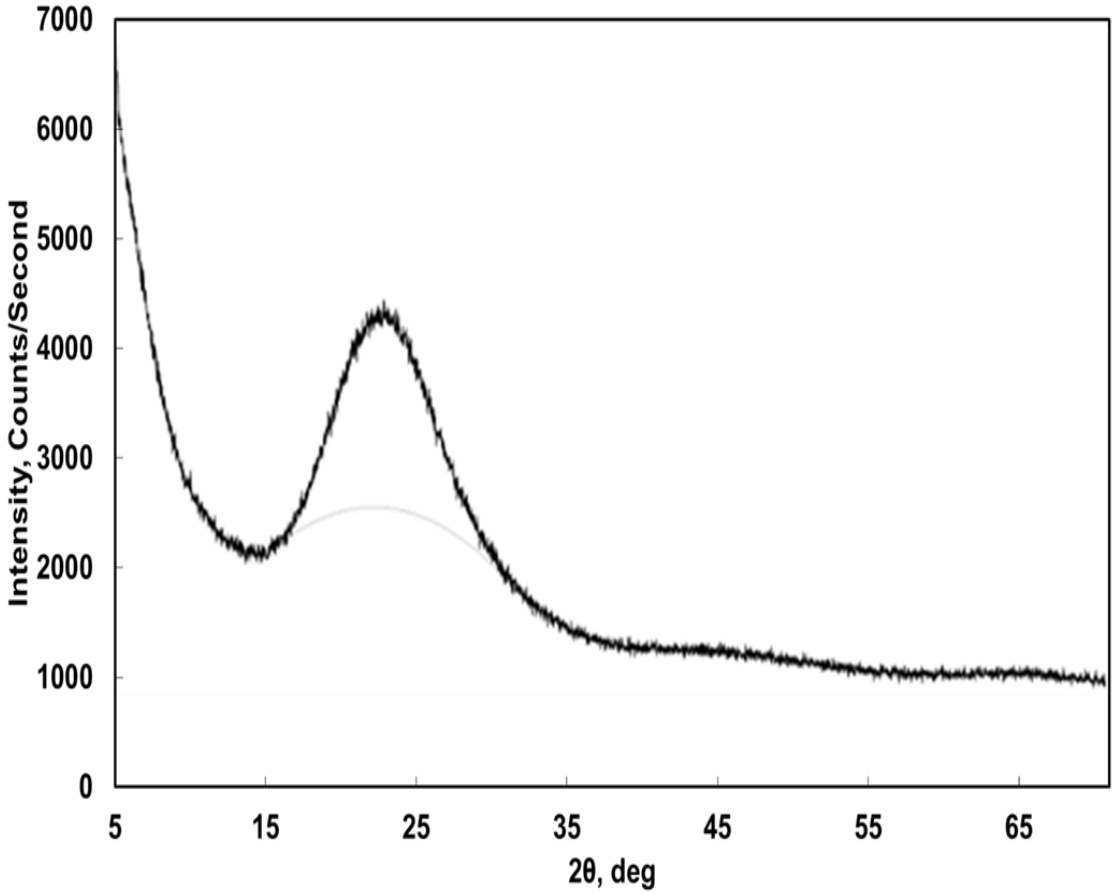

Fig. 3- XRD analysis of the prepared silica nanorods.

3.2 Iron Oxide Nanorods Analysis

The ironoxide nanorods were significantly smaller than their silica nanorod counterpart. The typical size of these rods were 50 nm by length and 15nm by diameter. The shape of these rods however are not uniform like the silica nanorods and had some deformation. The XRD analysis showed broad peaks of magnetite, maghamite, and goethite. The semi-qualitative analysis indicated the composition was 22 wt%, 32 wt%, and 44 wt%, respectively.

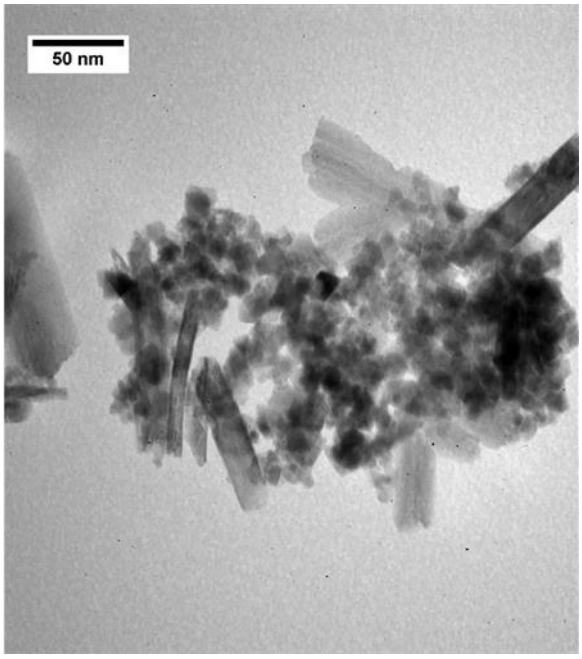

Fig. 4- TEM image of lab synthsized iron oxide nanorods.

Table 1- Iron oxide nanorod composition

Component	Concentration, wt%
Magnetite	23
Maghemite	22
Goethite	55

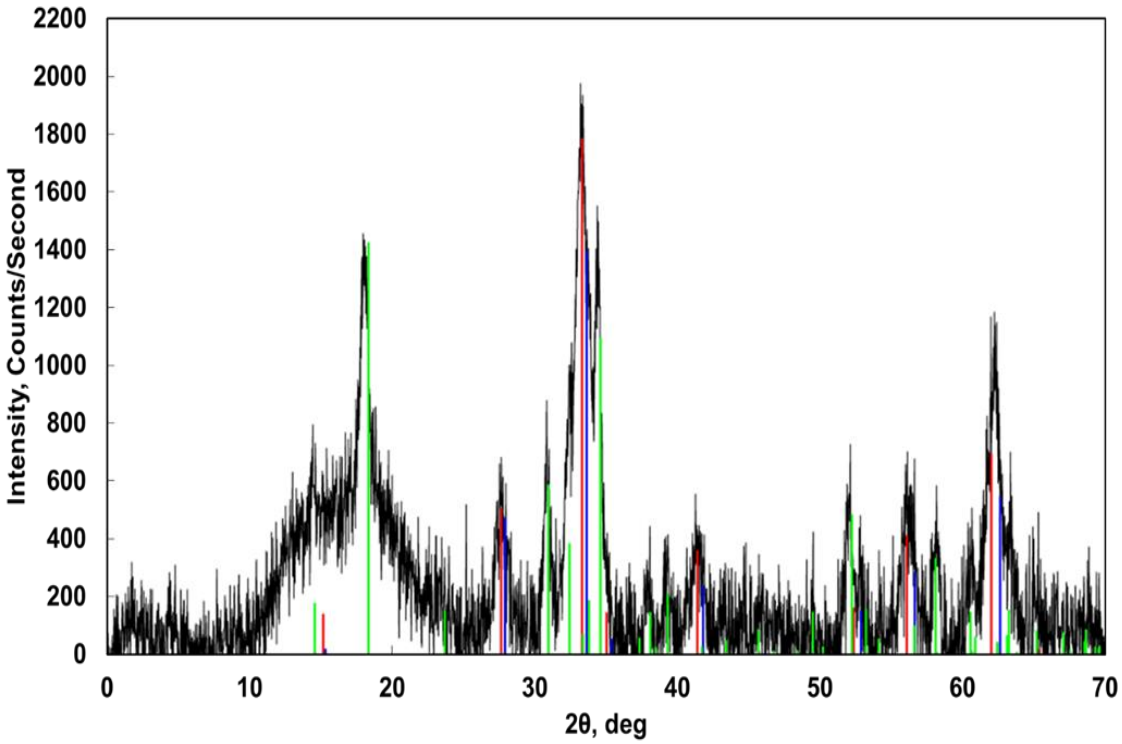

Fig. 5- XRD analysis of the iron oxide nanorods.

3.3 Silica Nanoparticle Analysis

The silica nanoparticles were also relatively large compared to its iron oxide counterpart. The average dominant size of the particle is typically at a range of 200 nm. The particles have a wide range of size typically form 100 nm to 1000nm. From the TEM images, the shapes of the particles appear to be perfect spheres. They also have a high tendency to aggregate.

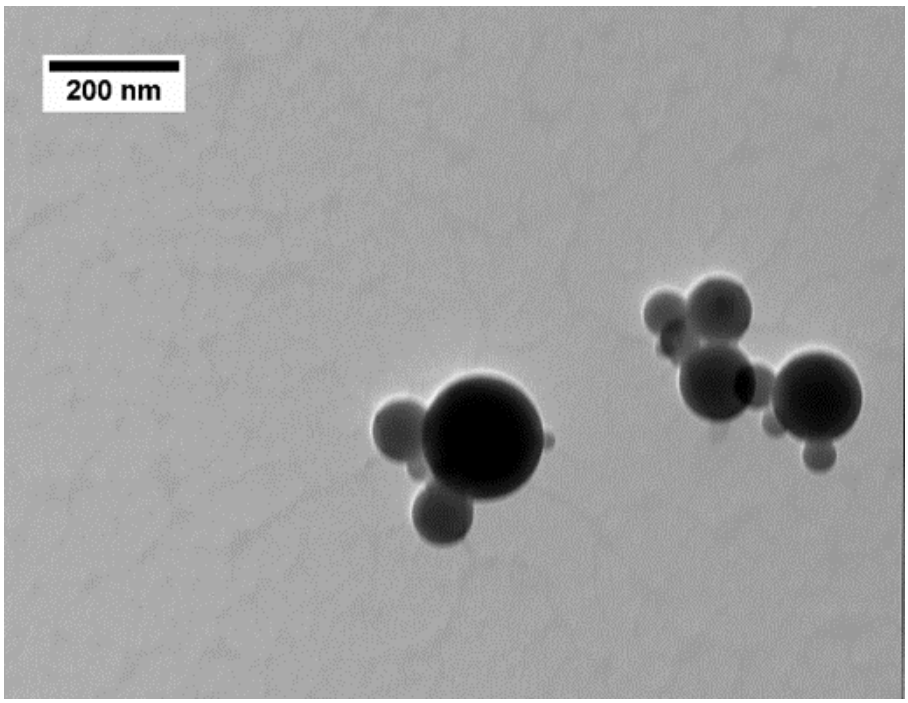

Fig. 6- TEM image of the silica nanospheres.

3.4 Iron Oxide Nanoparticle Analysis

The iron oxide nanoparticle size ranged from 90 to 300 nm with the majority of the particles' size being 150 nm. The shape of the particles are octahedral in nature and are uniform. The average hydrodynamic radius is 300 nm. From the zeta potential analysis, the particles were determined to be positively charged with a zeta potential of +10 mv.

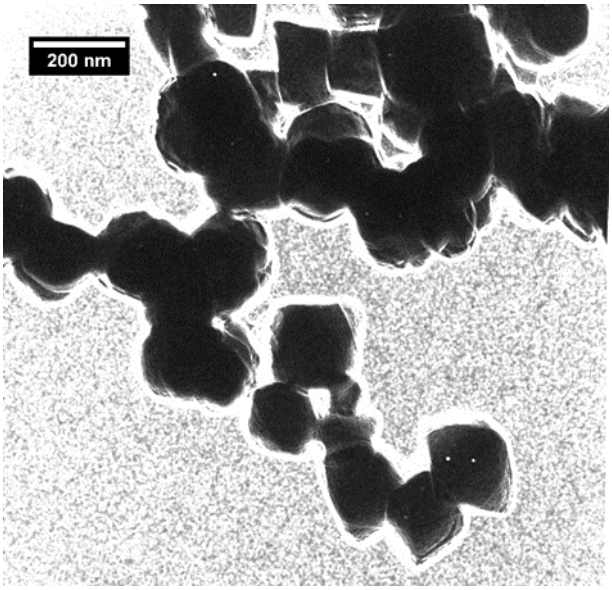

Fig. 7- TEM image of the octahedral iron oxide nanoparticles.

3.5 VES Zeta Potential Assessment and Particle Charge Impact

The zeta potential of different mixtures of nanoparticles, VES, and brine were determined. Dynamic light scattering (DLS) was used to determine the VES micelle size, the nanoparticles, and the VES-nanoparticle mixtures. Both the silica and iron oxide nanoparticles were dispersed in deionized water and were determined to be negatively positively charged, respectively. The average zeta potential values were -60 mV and +10 mV. The VES and $CaCl_2$ solution exhibited a negative zeta potential of -5 mv. Upon the addition of both silica and iron oxide nanoparticles separately, the zeta potential analysis yielded a neutral value. This indicated that the nanorods directly interacted with the VES and assisted in the screening of the VES head groups charge. The DLS analysis showed that before nanoparticle addition, the average micelle size was 600 nm, but after the addition of nanoparticles, the micelle size increased to 30 microns. These results indicate that multiple nanoparticles were incorporated in the micelle surface and that they contributed to micelle enlargement by adsorbing different micelles onto the same nanoparticle. The excessive enlargement of the micelle size is attributed to the large size of the silica nanorods and its aggregation to other silica nanoparticles.

Table 2- Zeta poetential and size assessment of silica nanorods in VES

7 pptg silica nanorods in 4 wt% VES in 23 wt% $CaCl_2$	**R_h, nm**	**PI**	**Zeta Potential, mV**
7 pptg Silica nanorods in deionized water	388	0.05	+60
4 wt% VES in 23 wt% $CaCl_2$ brine	673	0.22	-5
7 pptg silica nanords + 4 wt% VES + 23 wt% $CaCl_2$	30,000	15	-3 to 3

3.6 Particle Shape Impact on VES Rheology

The rheology tests were performed at 280 and 350ºF at 2 and 4 wt% of VES. A base solution was formulated at these two different concentrations without the presence of nanoparticles. The first two rheology tests were conducted with the presence of both types of silica nanoparticles at 4 wt% VES. The first rheology test was conducted with the nanorods and the second test was conducted with the nanospheres, at a concentration of 7 pptg. Fig. 8 presents the data comparing the performance of silica nanorods, nanospheres, and the VES solution containing no nanoparticles.

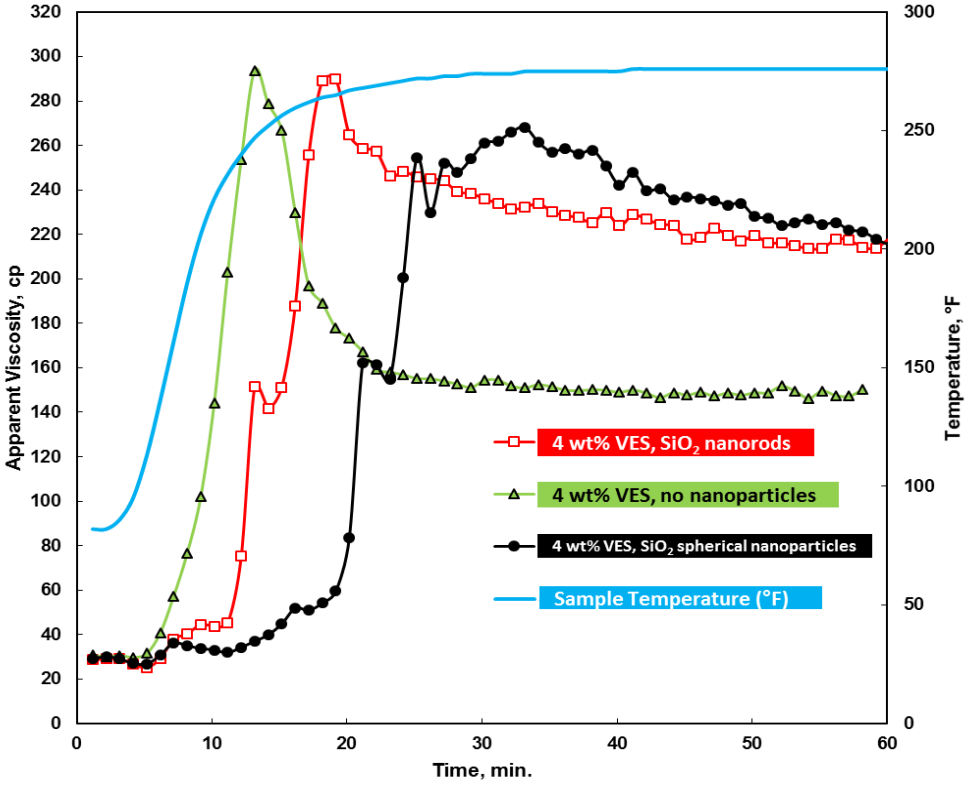

Fig. 8- The apparent viscosity of the 4 wt% VES base fluid compared to the fluids containing silica nanospheres and nanorods at 280ºF and shear rate 100s^{-1}.

The solution containing no nanoparticles held a viscosity of 150 cP for 1 hour. The solution containing the silica nanospheres obtained a peak viscosity of 260 cP and withheld a viscosity of 220 cP for 1 hour. And finally for the solution containing the nanorods, a peak viscosity of 300 cP was reached but it declined to 220 cP for 1 hour. From the results of these rheology tests, it is clear that the silica nanospheres and nanorods have a positive impact on the on the viscosity enhancement of the VES with the presence of $CaCl_2$. The solution containing the silica nanospheres however appears to exhibit a higher average of viscosity throughout the test, maintaining the viscosity around the region of 240 cP. Both tests indicate that the positively charged silica nanoparticles are compatible with the zwitterionic VES. The zeta potential analysis further indicates the additional screening to the surfactant head groups which further assisted in micellization. The increase of the apparent viscosity can be attributed to the VES micelles adsorbing on the silica nanoparticles' surface. The DLS analysis indicated this by showing the micelle enlargement of the solution. Because the silica nanorods and spheres were relatively large in size, heavy micelle entanglement on the particle surface increased the apparent viscosity.

Table 3- Viscosities of fracturing fluids at 280°F and 4 wt% VES, 100 s^{-1} (Silica nanoparticles)

Solution	Viscosity (cP)
VES	150
VES + Silica Nanorods	220
VES + Silica nanospheres	220

For the iron oxide nanoparticles, no enhancement was observed when they were in solution with the VES, as shown in Fig. 9.

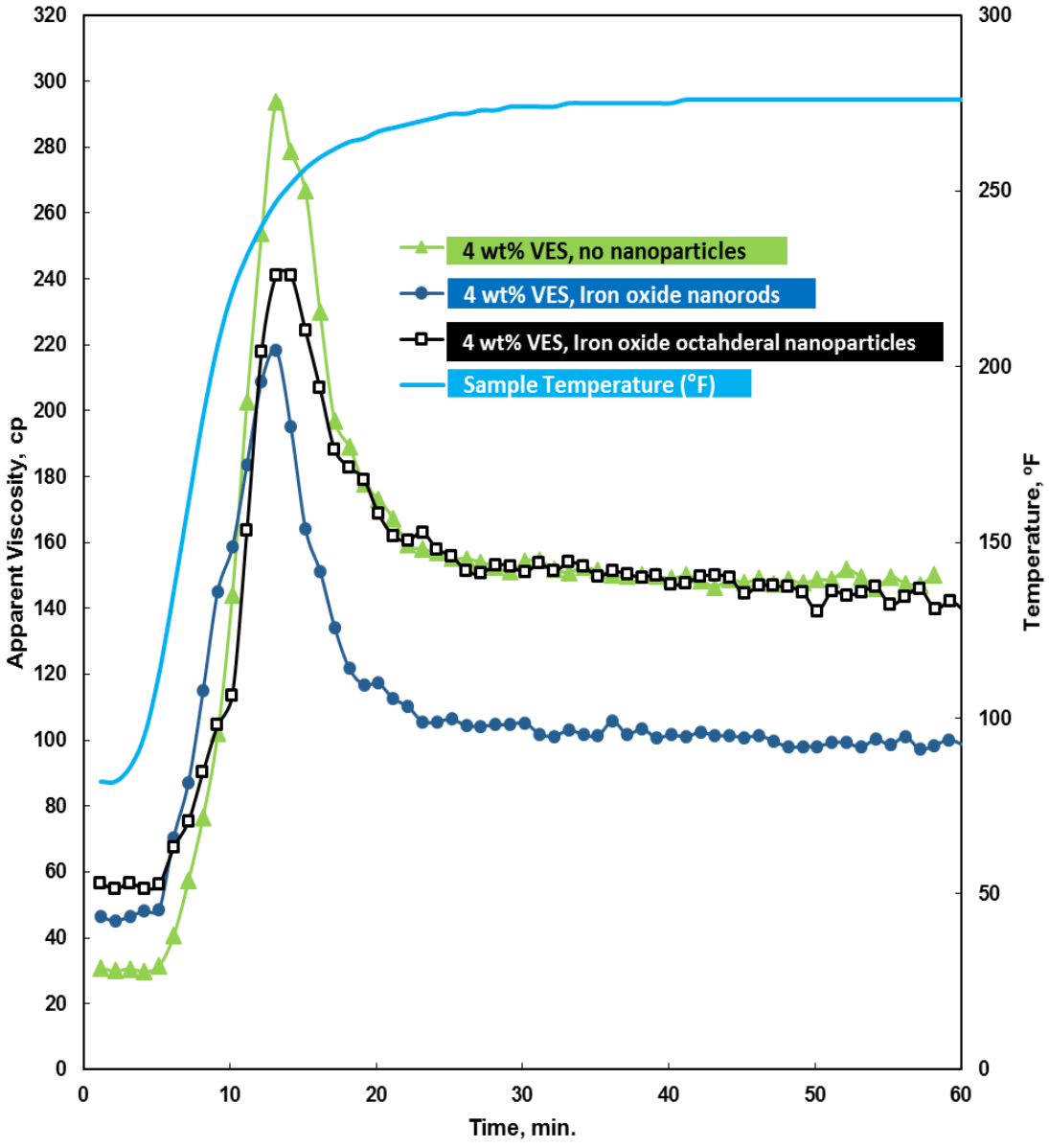

Fig. 9- The apparent viscosity of the 4 wt% VES base fluid compared to the fluids containing iron oxide nanospheres and nanorods at 280ºF and shear rate 100s^{-1}.

The nanospheres do not contribute to any viscosity enhancement of the VES system. It achieved a maximum of 240 cP and withholds at 150 cP for 1 hour upon heating. The nanorods contributed negatively, and a maximum viscosity of 220 cP is achieved and the system plateaus to 100 cP upon heating as well. These results indicate that the varying shapes of the iron oxide nanoparticles fail to enhance the micellization of the solution.

Table 4- Viscosities of fracturing fluids at 280°F and 4 wt% VES, 100 s^{-1} (Iron oxide Nanoparticles)

Solution	Viscosity (cP)
VES	146
VES + Iron oxide nanorods	98
VES + Iron oxide octahedral nanoparticles	146

To examine the effectiveness of both types of nanoparticles on enhancing the micellization process, the concentration of the VES was reduced to 2 wt%, and the temperature was still maintained at 280°F. A new base fluid was formulated as well and the apparent viscosity measured to be 70 cP, much lower than the viscosity of the 4 wt% VES system. The silica nanorods was found to be the best type of nanoparticle to enhance the micellization process. The apparent viscosity achieved was 100 cP and was maintained for 1 hour. After an additional hour though, the viscosity decreased to 70 cP, and maintained that value. Since there was a lower concentration of VES in an environment of relatively high concentration of nanoparticles, which are oppositely charged, more adsorption of the micelles on the nanoparticles occurred. This formed a bilayer structure,

which can explain the loss of rheology in the second hour of the test. This further implies that the higher the concentration of VES, wormlike micelles are maintained and the system avoided formation of the bilayer on the silica nanorods.

In the case of the iron nanorods, the system achieved a viscosity of 140 cp and then plateaud to 65 cp by the end of the hour. It achieved a viscosity higher than the silica nanorods however it declined faster than the silica nanorod system. Despite achieving high viscosity, the silica nanorod system out-performed the iron oxide nanorod system. Based off of the rheology graphs it can easily be deduced that both types of nanorods and nanospheres starts the micellization process at lower temperatures later than the systems without them. This can be attributed to the elongated cylindrical shape of both nanorods. The adsorption process of the micelles on the nanorods occurs and bridging between the dispersed micelles is formed creating a complex network of micelle-micelle entanglement. Both systems containing the silica and iron oxide nanorods indicated that the decay rate of the viscosities is greatly reduced compared to the VES system containing no nanorods when operating for 1 hour at 280°F.

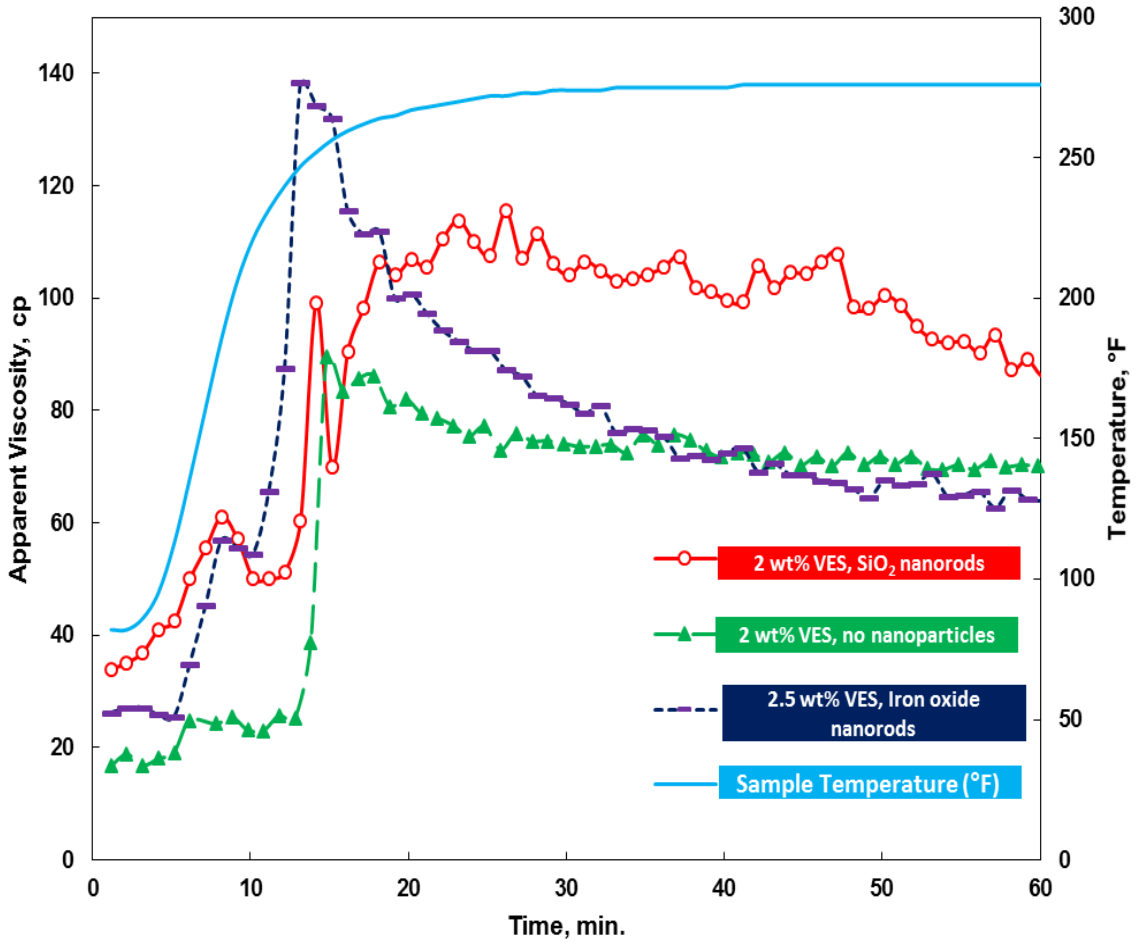

Fig. 10- The apparent viscosity of the 2wt% VES base fluid compared to the fluids containing silica nanorods and iron oxide nanorods at 280°F and shear rate 100s^{-1}.

Despite the fact that both silica and ironoxide nanospheres either enhanced the viscosity of the VES system or had no significant effect at 4 wt% VES, both types of nanospheres had a negative impact on the performance of the VES at 2 wt%. Upon addition of silica nanoparticles in the VES, the maximum viscosity achieved was 20 cp and as heating continued to occur, the viscosity dwindled down to 5 cp at 280°F. Similar phenomena occurred with the iron oxide nanosphere system. The viscosity this time

increased to 30 cP but by the time the temperature hit 280°F, the viscosity decreased to 2 cP. It can be deduced that since there was a smaller concentration of VES, most of the surfactant was adsorbed on the nanosphere surface preventing any micellization from occurring. Given that no or very little micellization occurred, there was no micelle-micelle entanglement, which could generate viscosity.

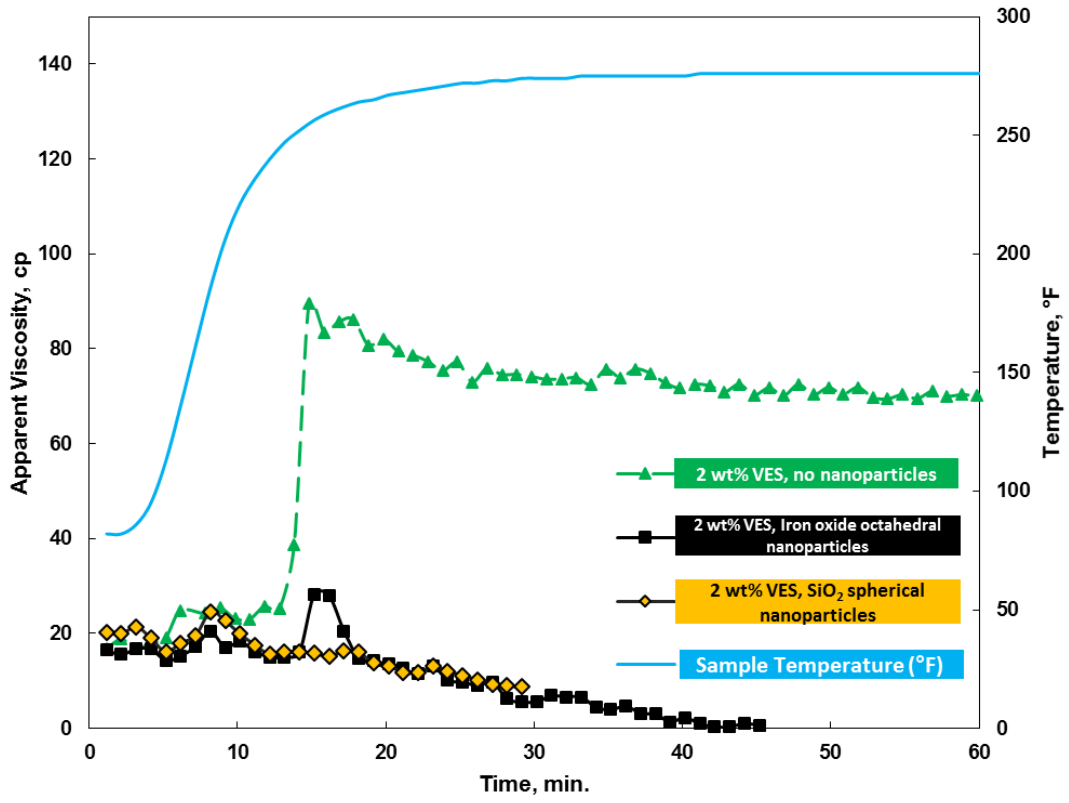

Fig. 11- The apparent viscosity of the 2 wt% VES base fluid compared to the fluids containing silica nanospheres and octahedral iron oxide nanoparticles at 280ºF and shear rate 100s^{-1}.

Table 5- Viscosities of fracturing fluids at 280°F and 2 wt% VES, 100 s^{-1} (All Nanoparticles)

Solution	Viscosity (cP)
VES	70
VES + Silica nanorods	87
VES + Iron oxide nanorods	65
VES + Silica nanospheres	6
VES + Iron oxide octahedral nanoparticles	2

Given all the findings from the rheology tests at 280°F, this work proceeded to test the performance of all the nanoparticles on VES at a higher temperature of 350°F. The concentration of VES however was only tested at 4 wt% because at high temperatures, small concentration of VES is not stable enough to produce micellization and significant viscosity.

For the first part of this section, the silica nanorods were added to the anionic VES system containing the $CaCl_2$ brine and showed an enhancement in apparent viscosity. The highest value reached was 180 cP, which occurred at 300°F. It then gradually decreased 140 cP at 320°F, and decreased to 57 cP at 350°F. After 50 minutes, the viscosity decreased to 51 cP and then dropped to 40 cP.

The performance of the silica nanospheres was very similar compared to the silica nanorods at 350°F, but ultimately they achieved a greater enhancement of the viscosity of

the VES system. Fig. 12 indicates that peak viscosity was 230 cP at 310^{o}F and gradually declined to 180 cP at 330^{o}F. It finally reached a value of 100 cP when the temperature reached 350°F. After 1 hour of additional heating at 350^{o}F, the viscosity decreased to 75 cP.

The addition of iron nanorods, however, showed no enhancement to the viscosity of the system and a negative impact on it. The results displayed in Fig. 12 shows that the viscosity of the VES system containing no nanoparticles could not withstand the 350^{o}F environment, and could not maintain at 50 cP once that temperature was reached. The maximum viscosity ever achieved was 140 cP, which was half the value of that of the 280^{o}F experiment. Once the temperature reached 350^{o}F, the viscosity decreased to 10 cp, which indicated poor rheological performance. The iron oxide nanorod performance at 350^{o}F behaved oppositely to the test conducted at 280^{o}F. The maximum apparent viscosity was 200 cP at 280^{o}F which then decreased to 160 cP at the same temperature. For the 350^{o}F rheology test, the viscosity increased to 210 cP at 300^{o}F but slowly decreased to 85 cP at 350^{o}F. Upon further heating at the same temperature for 1 hour, the viscosity decreased to 45 cP.

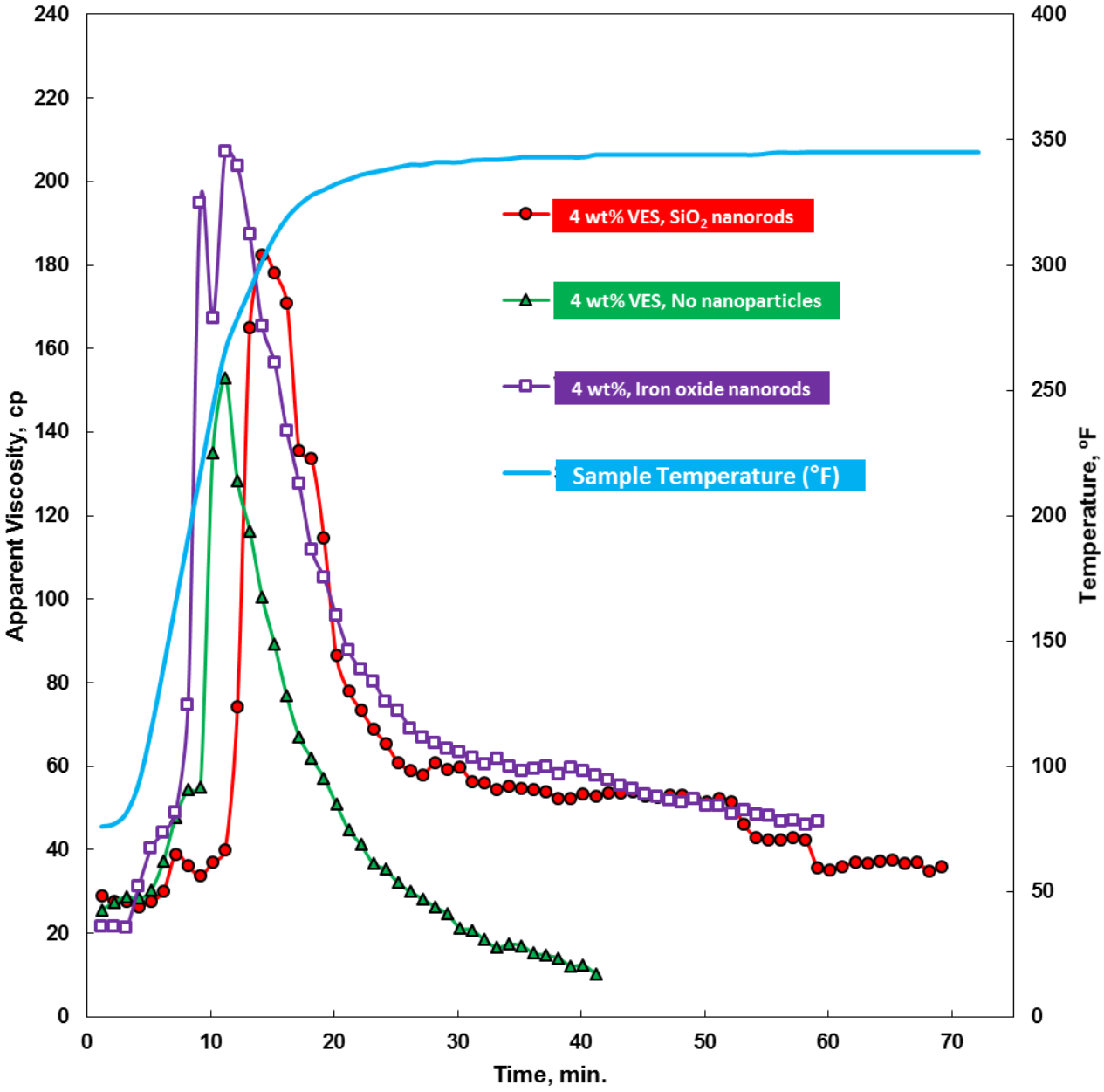

Fig. 12- The apparent viscosity of the 4 wt% VES base fluid compared to the fluids containing silica nanorods and iron oxide nanorods at 350°F and shear rate 100s^{-1}.

The greatest VES system performance at 350^{o}F was observed to be the system that contained the iron oxide octahedral nanospheres. Fig. 13 displays its rheological performance and shows that the maximum viscosity reached was 240 cp at 280^{o}F. It then gradually declines to 100 cp by the time the system reaches 350^{o}F and maintains a viscosity of 90 cp for 1 hour.

Based off of this analysis, all the nanoparticles exhibited good thermal stability for at least 1 hour. Since there is opposite behavior for the silica nanoparticles and the iron oxide nanorods at 350^{o}F, compared to the behavior at 280^{o}F, it can be deduced that temperature controls the mechanism of nanoparticle-micelle interaction. Also, the

nanosheres of both silica and iron oxide showed the greatest positive impact on the viscosity of the VES system at 350°F.

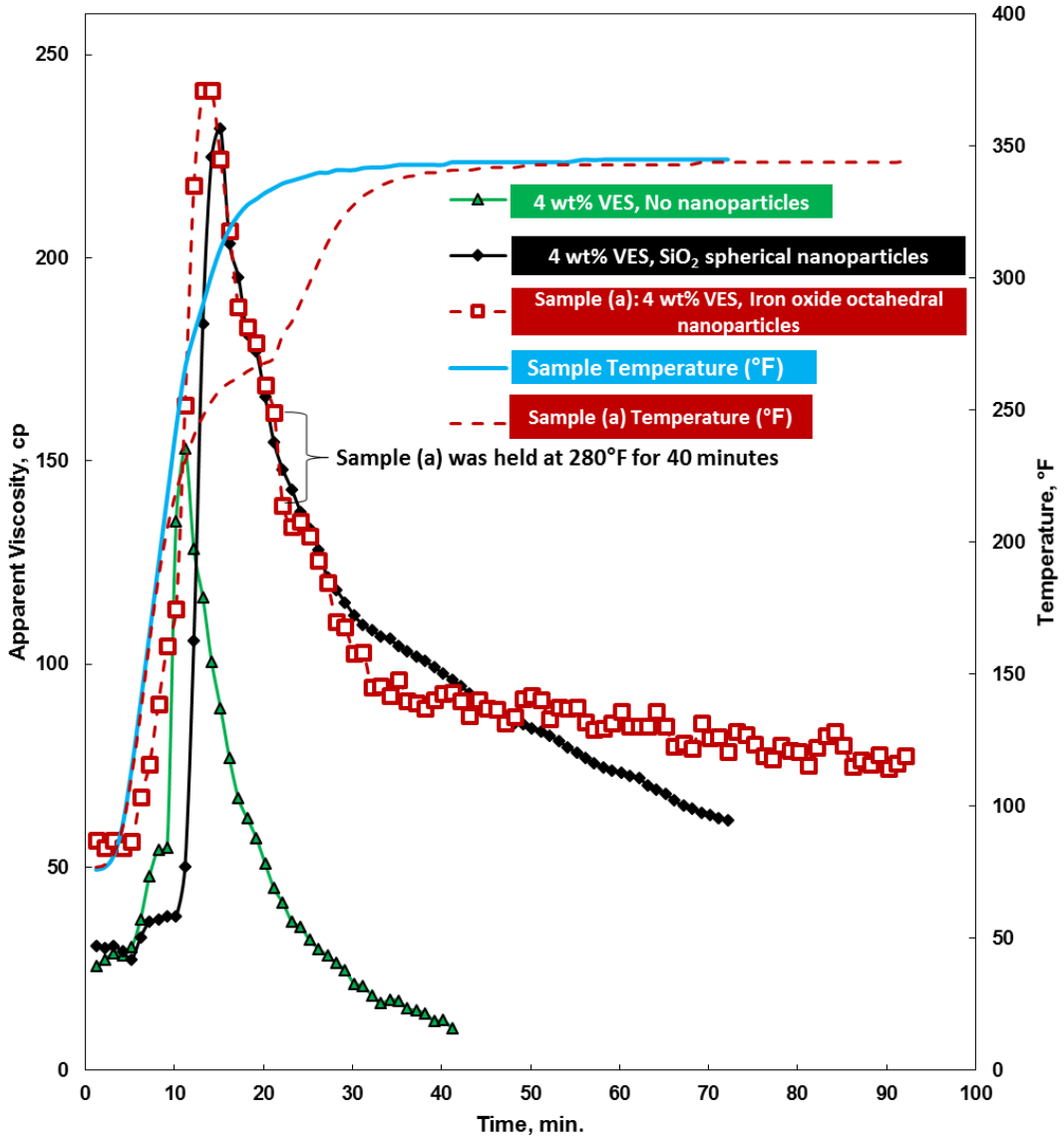

Fig. 13- The apparent viscosity of the 4 wt% VES base fluid compared to the fluids containing silica nanospheres and iron oxide octahedral nanoparticles at 350°F and shear rate 100s^{-1}.

Table 6- Viscosities of fracturing fluids at 350ºF and 4 wt% VES, 100 s^{-1} (All Nanoparticles)

Solution	Viscosity (cP)
VES	10
VES + Silica nanorods	36
VES + Iron oxide nanorods	47
VES + Silica nanospheres	62
VES + Iron oxide octahedral nanoparticles	85

3.7 Microscopic Study

All of the fracturing fluid samples were examined under an optical microscope to observe aggregate behavior and dispersal. The before and after rheology tests performed at 350°F specifically were observed. It can be seen from Fig. 14, that before heating, the silica nanorods-VES mixture displayed large and randomly shaped surfactant aggregates. Smaller surfactant aggregates were observed and appeared to be elongated. Observing the after heated samples, the amount of aggregates reduced with no change in orientation and shape.

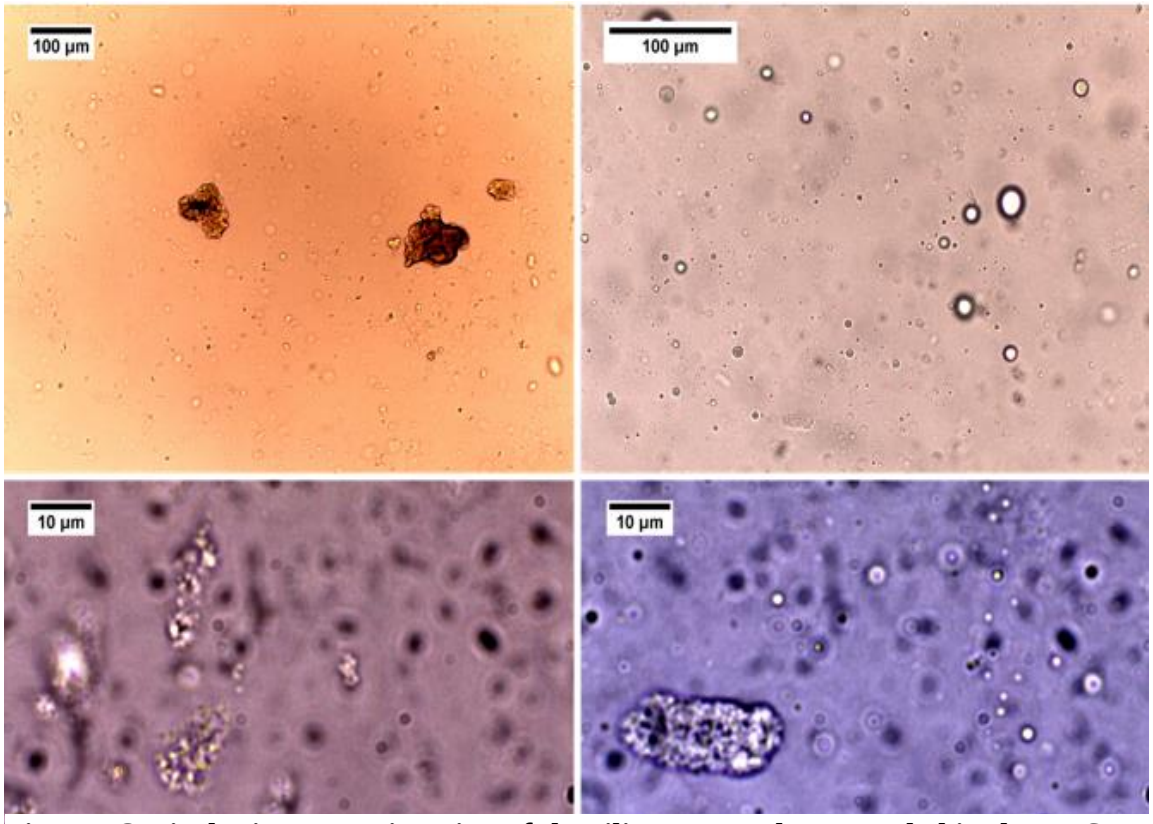

Fig. 14- Optical microscope imaging of the silica nanorods suspended in the VES, before and after. At moderate magnification, the image shows randomly shaped surfactant with nanoparticles. At higher magnification, elongated surfactant aggregates are shown which are smaller than the randomly shaped surfactant in the lower magnification images.

Fig. 15 displays the before and after images of the samples that contained the silica nanospheres. The observed surfactant aggregates were also large and randomly shaped. After heating, the shapes of the aggregates appeared to be string-shaped and elongated. They were present in vast amounts and their orientation was random.

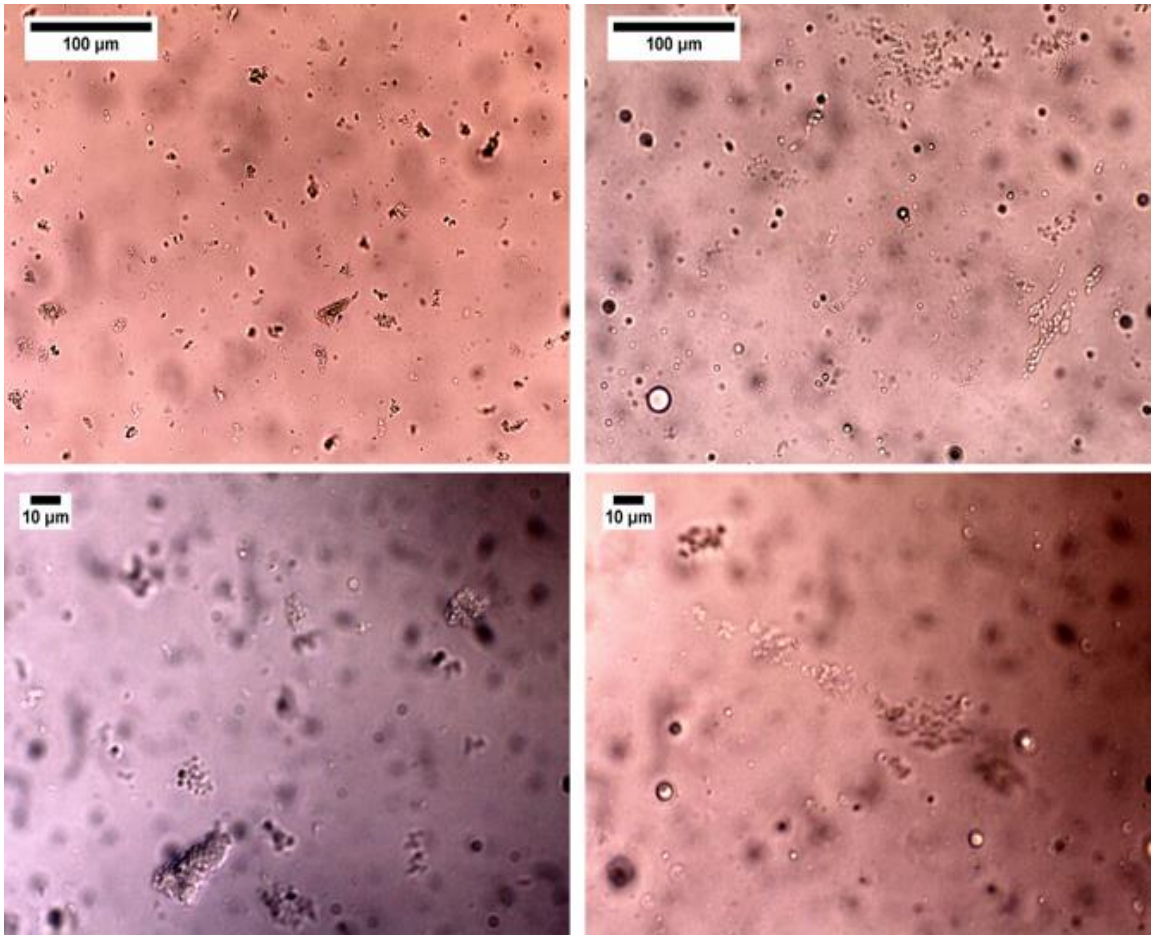

Fig. 15- The moderately magnified images shows randomly-shaped surfactants with nanoparticles dispersed. After heating, the moderate magnification shows some monodispersed surfactant aggregates. With high maginification, the aggregates seem to have elongated.

Examining the iron oxide nanorod specimens, the microscopy images showed that the aggregates were also randomly-shaped. They appeared to aggregate heavily on the randomly shaped surfactant bodies. Fig. 16 shows that upon heating, the nanorods became uniformly dispersed and finer. With higher magnification, the surfactant bodies displayed discontinuity and no specific orientation and shapes.

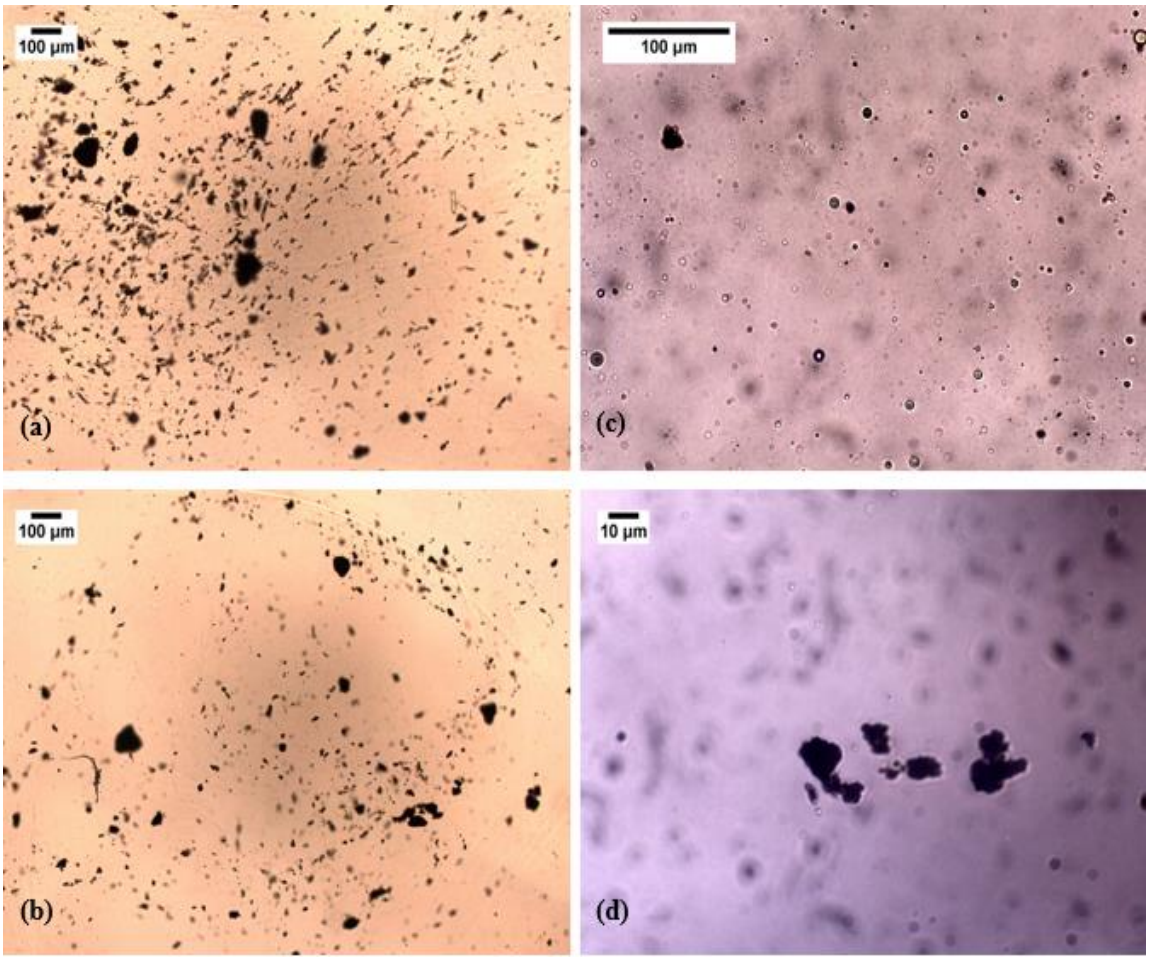

Fig. 16- Before (A and B): Zwitterionic surfactant and iron oxide nanorod aggregates that are randomly shaped and polydispersed. After (C and D): Aggregates are smaller than what they were before heating.

Fig. 17 shows the behavior of the surfactant bodies and iron oxide octahedral nanoparticles. The nanoparticles were embedded in the surfactant bodies and were uniformly dispersed throughout the solution. They also displayed uniform and a defined orientation. The iron oxide nanoparticle-surfactant complexes displayed a needle-shape appearance of lengths up to 100 microns. However, after heating, the needle-shaped complexes decreased to 5 microns and maintained their shapes.

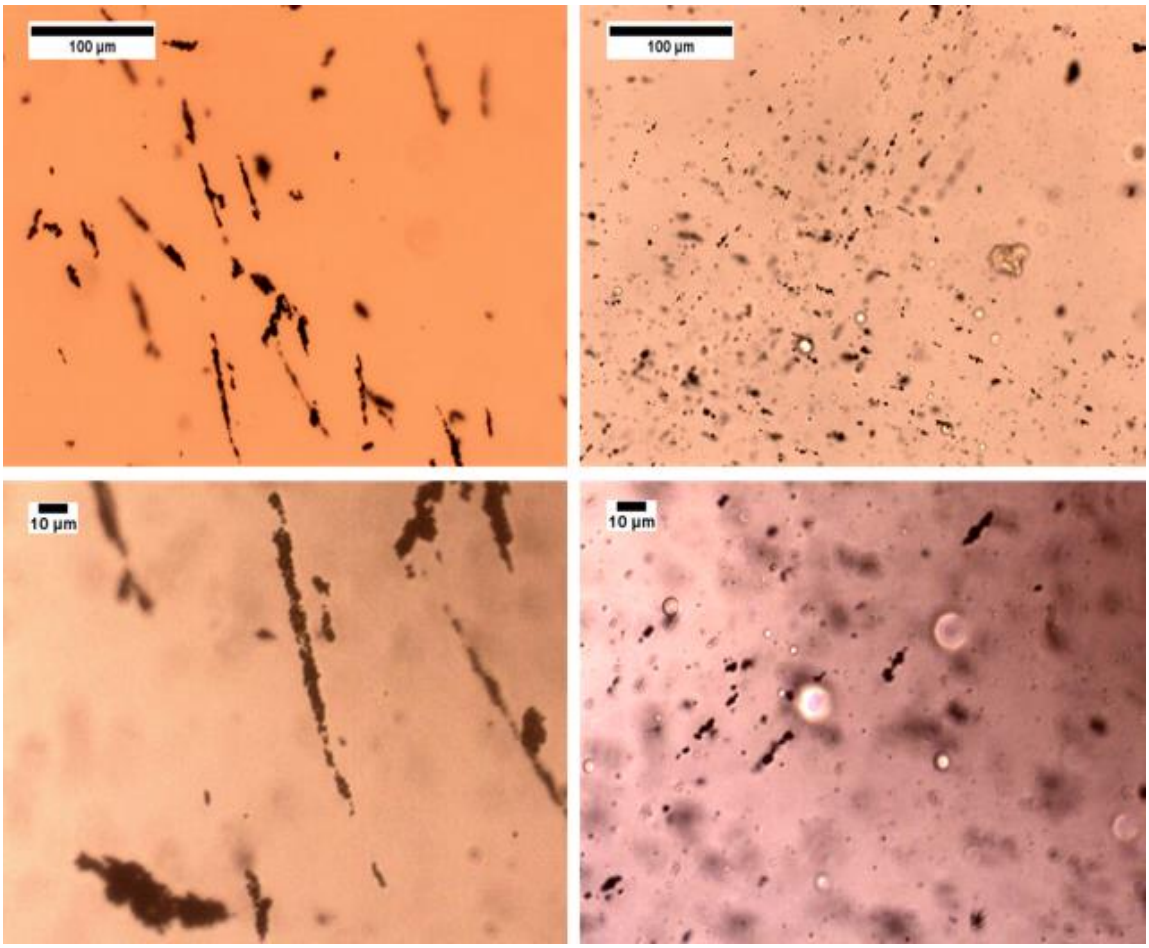

Fig. 17- Before (A and B): Lower magnification shows needle shaped surfactant aggregates that are monodispersed and have uniform orientation. After heating (C and D): Lower magnification shows particles that are polydispersed and have nonuniform orientation. High magnification show a decrease in size of the surfactant aggregates.

This same sample was observed under TEM after being heated to 350°F. Fig. 18 displays the TEM image and it can be observed that the nanoparticles clustered together and were bonded together by the VES. The needle-shaped nature of the surfactant bodies can be attributed to the closely packed nanoparticle clusters. At higher magnification, it can be observed that there are 8 octahedral nanoparticles connected to each other with the VES encapsulating them. Pseudo crosslinking of the surfactant body and the nanospheres occurs and yields this large needle shaped mass. The dimensions of the body are 650 nm in length and 200 nm in width. It can be deduced that this interaction explains the extension of thermal stability during the rheology tests.

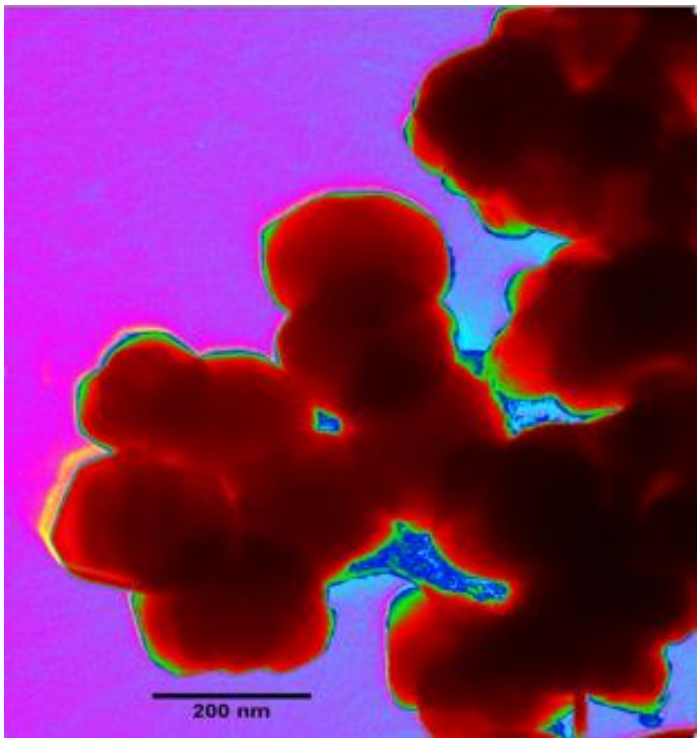

Fig. 18- TEM image of ironoxide octahedral nanoparticles being engulfed by zwitterionic VES at room temperature. This illustrates the reason why needle shaped aggregates formed.

Since both the silica and iron oxide nanopsheres are of large nature (200 nm), it can be concluded that they cause the surfactant bodies to elongated compared to their nanorod counterparts. Both samples containing the nanospheres exhibited the highest apparent viscosities and thermal stability at 350°F. This behavior can be attributed to the nanoparticles aggregation in the surfactant and forming the structures observed earlier in the microscopic images. Since the silica and iron oxide nanorods ranged in 50 to 300 nm in size, they produced smaller spherical surfactant bodies, which displayed lower apparent viscosity and thermal stability at 350°F.

3.8 Micelle Size and Nanoparticles' Performance

A trend can be drawn that can describe the impact of the nanoparticle shapes on VES from the data produced from the rheology tests that were conducted with varying VES concentration and varying temperatures. Keeping the $CaCl_2$ concentration constant and decreasing the VES concentration from 4 to 2 wt%, increases the ratio between salt to VES. This leads to the formation of longer wormlike micelles. Because the wormlike micelles are larger, this results to less amount of micelle head groups. The micelle head groups act as connection points between the wormlike micelles and the surfactant layer adsorbed on the nanoparticles (Pletneva et al. 2015). Multiple publications have observed similar observations that have to do with the impact of salt concentration to VES ratio on micelle growth. Since higher salt concentration lowers the amount of head groups present by over growing the micelles, this leads to micelles to undergo nanoparticle adsorption equilibrium, which increases the connection probability (Helgeson et al. 2010). The higher the number of micelle head groups present leads to higher amount of micelle to

nanoparticle conjunctions, which increases the effect and impact nanoparticles presence have on the micelle crosslinking process.

Fig. 19 displays the effect of salt to VES concentration ratio and summarizes what nanoparticle species perform best in different conditions. Each data set were divided into three categories with category 1 being the long micelles, 2 being the moderate length micelles, and 3 being the branched micelles. The size of the micelles were predicted from the salt to VES concentration ratio and the maximum temperature of the rheology test. The 2 wt% VES at 280^{o}F resulted in the longest micelles, while the 4 wt% VES at the same temperature resulted in the moderate length micelles. Finally, the 4 wt% VES at 350^{o}F resulted in the branched micelles. From the plot, it can be deduced that the addition of the spherical silica nanoparticles and the octahedral iron oxide nanoparticles in 2 wt% VES resulted in a negative impact on the apparent viscosity of the VES. This result can be explained by the high surface area of the spherical and octahedral nanoparticles; they adsorb most of the VES into a bi-layer micelle-structure and deny the ability of the mixture to form enough wormlike micelles to generate sufficient viscosity. The overgrowth of the remainder surfactant in long worm-like micelles reduced the amount of available head groups which therefore quashed the ability of the nanoparticles to crosslink the micelles. The spherical and octahedral nature of the particles limited the VES' ability to form multiple micelles. They aggregated due to excessive screening of their charged head groups because of the significantly high salt concentration. However, the silica and iron oxide nanorods worked positively at this low VES concentration and this can be attributed to the elongated nature of these nanorods. The nanorods succeeded in connecting the long

and large micelles, which formed heavily crosslinked networks, which generated sufficient apparent viscosity.

At a higher concentration of VES and maintaining the same calcium chloride concentration of 23 wt% at 280^{o}F, the micelles were shorter in nature. The shorter micelles resulted in higher number of head groups as mentioned before, and this resulted in easier formation of micelles and micelle-particle crosslinking. From the rheological analysis of all the nanoparticles, both the silica and iron oxide spherical nanoparticles and nanorods resulted in similar enhancement of the viscosity of the zwitterionic VES. The increase in the number of crosslinking sites on both nanorods and spheres connected to the micelle head groups, which resulted to efficient and higher amount of crosslinking.

For the iron oxide nanoparticles, the octahedral nanoparticles were able to achieve crosslinking of the micelles and connect to each other which formed stronger and longer micelle networking as shown in the TEM images. The iron oxide nanorods however behaved differently; their small size resulted in excessive adsorption of the VES and insufficient head group attachment to the adsorbed layer. This can be explained by the oversaturation of the surface and completion between the head groups on the particle surfaces. This phenomena resulted in discontinuation of micelle network formation and a drop in rheological performance.

From literature, it was reported that increasing the temperature significantly to higher ranges can be major factor of decreasing the size of micelles and leading them to have branched structures. It also leads to an increase in the amount of micelle head groups. This theory compliments the rheological performance of the iron oxide octahedral

nanoparticles and silica spherical nanoparticles in terms of achieving a viscosity and sustaining it higher than 75 cp for more than 1 hour at 350^{o}F.The increase in the number of head groups helped the saturation of the nanoparticle surface with the micelle head groups which resulted in higher thermal stability and stronger inter-micellar pseudo-crosslinking. At 350^{o}F, the solutions' apparent viscosities containing both types of nanorods plateaued, but succeeded in achieving a viscosity of higher than 50 cp for hour. This moderate success is attributed to the saturation of the nanoparticles' surface by available micelle head groups, which made the branching of the head groups in valuable due to geometrical limitations of the nanorods, which provided less access points on their surfaces.

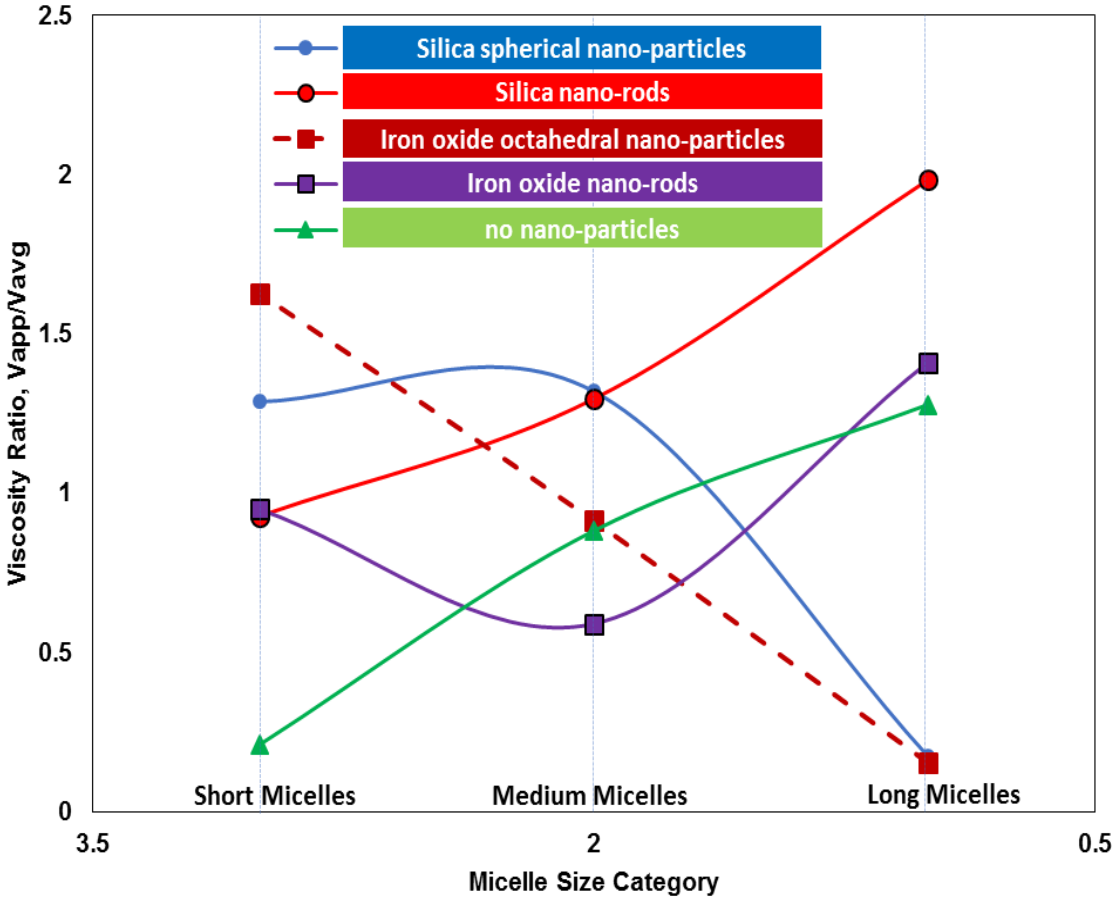

Fig. 19- Micelle length relation. Long micelles: 2 wt% VES at 280ºF. Medium micelles: 4 wt% VES at 280ºF. Short micelles: 4 wt% VES at 350ºF.

3.9 Cation Type and Concentration Impact on VES Micelles Entanglement

This work further examined the impact of different types of brine and their compositions on the VES response to the silica nanospheres. The monovalent salt chosen to compare with $CaCl_2$ was NaCl. Both fracturing fluids were prepared with 10,15, 23 wt% salt concentration, with 4 wt% VES and 7 pptg silica nanospheres added to them. The fracturing fluids were rheologically evaluated at a shear rate of 100 s^{-1} and at 280ºF.

The increase in $CaCl_2$ concentration from 10 to 15% had a minimal impact on the apparent viscosity of the VES as shown in Fig. 20. However, increasing the $CaCl_2$ concentration to 23 wt% raised the apparent viscosity from 90 to 200 cp. When examining the impact of the Na^+ ions at the same concentration, the performance of the fracturing fluid drops significantly. Fig. 21 displays the performance and the initial viscosity of 28 cp decreases to 0 cp after 10 minutes, which signifies severe deterioration in fracturing fluid viscosity. However, when decreasing the concentration of NaCl to 15 wt% and 10 wt%, the apparent visicosity of the fracturing fluid increased. The apparent viscosity increased from 0 to 85 cp and 50 cp, respectively, which signifies a positive impact. This can be explained by two factors: the monovalency of the cation and the decrease of concentration; they both alter the packing factor of the VES, thus transforming the micelle entanglement arrangement. These transformations vary between short and long wormlike micelles, and spherical and bi-layered micelle geometries.

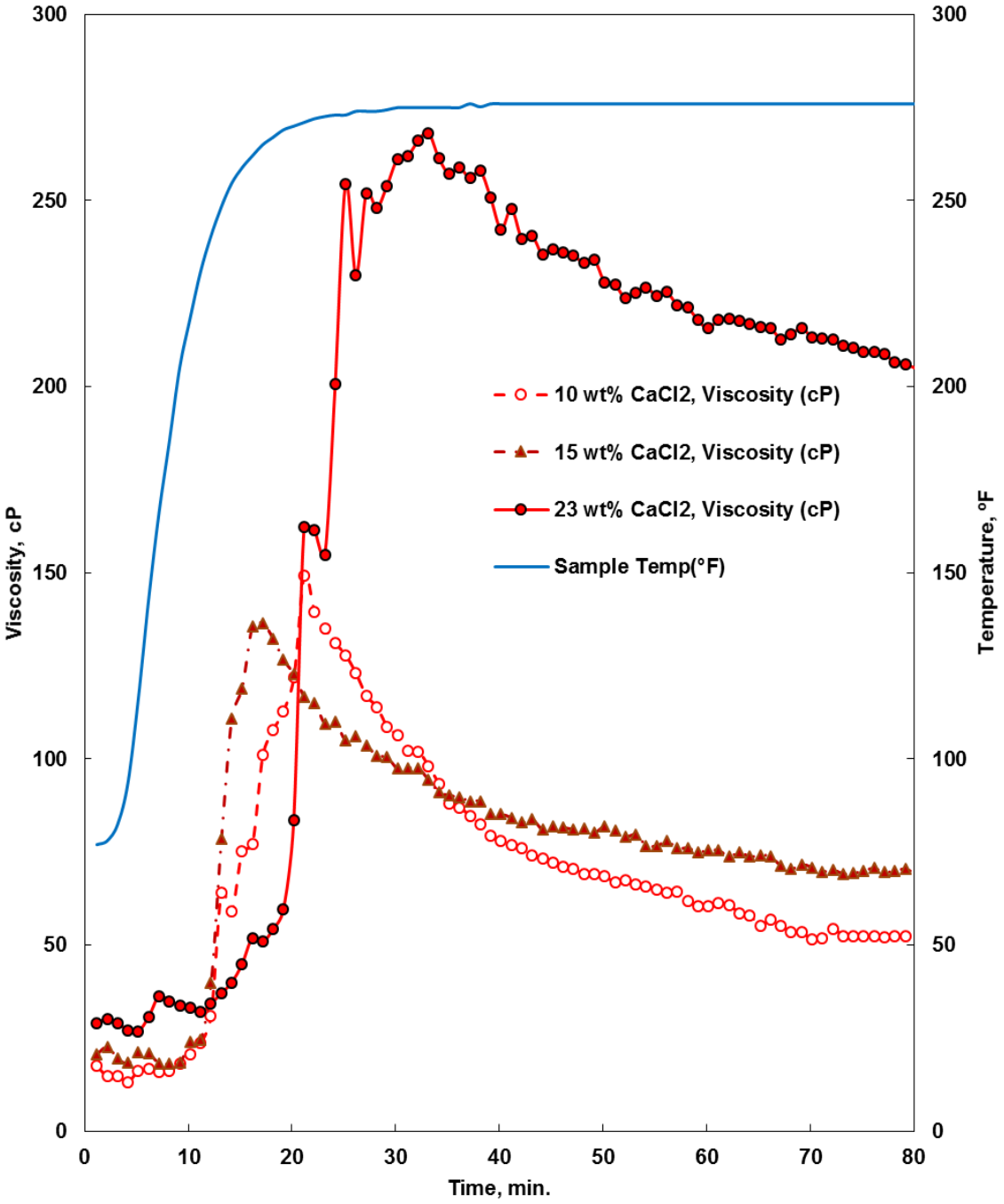

Fig. 20- Apparent viscosity of VES using various concentrations of $CaCl_2$ brine in 4 wt% VES and 7 pptg silica nanospheres. The operating conditions were at 280°F and at 100 s^{-1}.

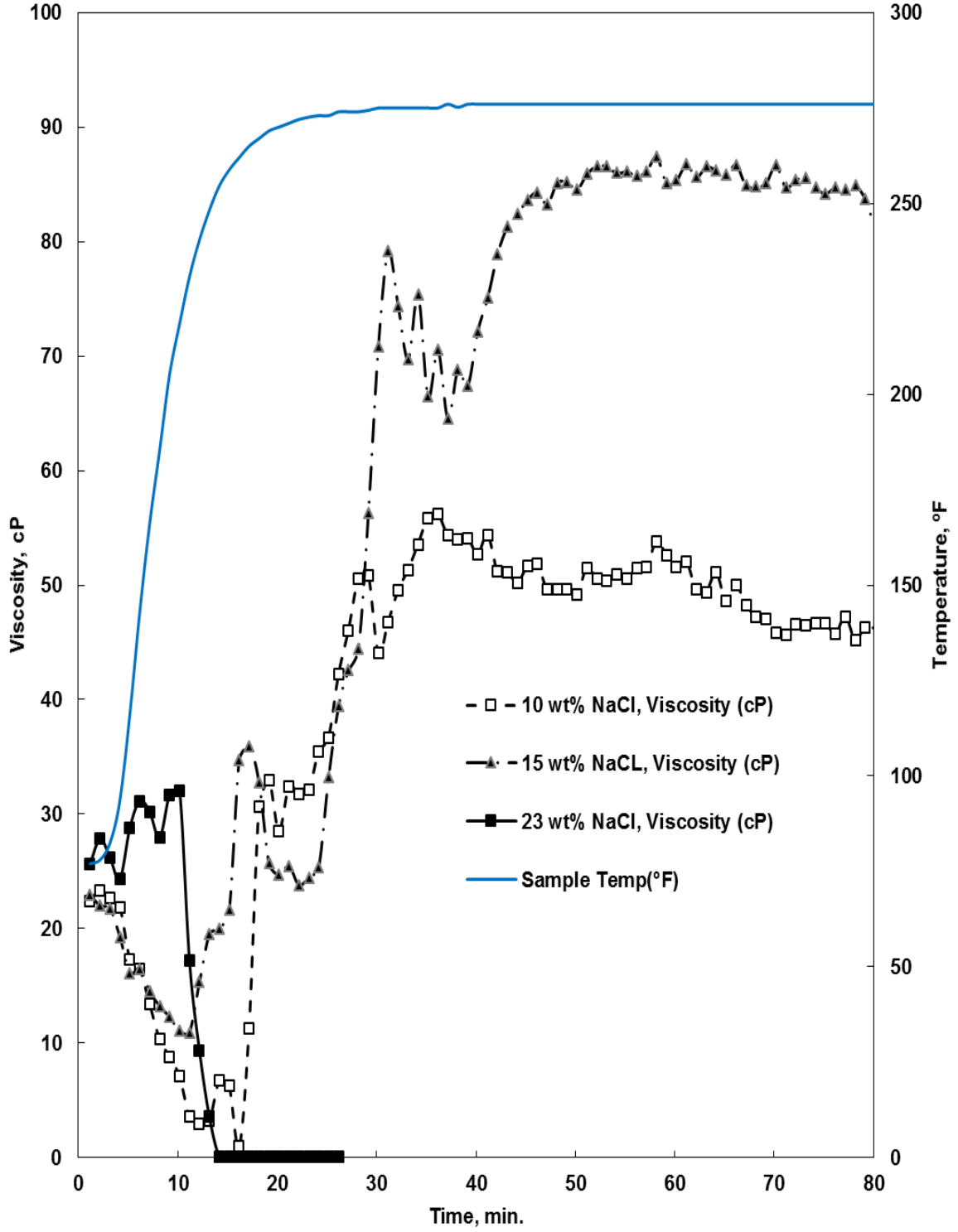

Fig. 21- Apparent viscosity of VES using various concentrations of NaCl brine in 4 wt% VES and 7 pptg silica nanospheres. The operating conditions were at 280°F and at 100 s^{-1}.

3.10 Dynamic Oscillatory Measurement

Dynamic oscillatory measurement (DOM) was used to evaluate the impact of nanoparticle shape and type on the proppant carrying capacity of the fracturing fluids. The DOM involved amplitude sweeps draw out the linear behavior zones. This was then followed by a frequency sweep to evaluate the microstructure of the VES (Gomaa et al., 2015). The storage and loss moduli of the fracking fluids containing nanoparticles and containing none were evaluated at 50% strain and at 280^{o}F. Fig. 22 illustrates the inversion of a fluid displaying viscous dominant behavior to elastic dominant behavior which occurs at a frequency of 1.2 rad/s corresponding to a relaxation time of 0.83s. The maximum value of G' and G" were 26 and 4.2 Pa, respectively. All of these characteristics show that the VES possess adequate elastic properties that have the ability to suspend proppants. Adding silica nanorods and nanospheres increased the value of the storage and loss moduli by 100 times the original values of the fluid containing no nanoparticles. The increase of G' and G" indicates higher degree of micelle-micelle entanglement and crosslinking (Knoll and Prud'homme 1987). The silica nanospheres and nanorods not only increased the values of G' and G", but also maintained a G' higher than G". The silica nanoparticle enhanced fracturing fluids also experienced an increase in relaxation time compared to the stand alone VES fluid. Comparing the silica nanorods performance to its nanosphere counterpart, the nanorods exhibited less enhancement in relaxation time reaching 1s compared to 1.3s with the nanospheres.

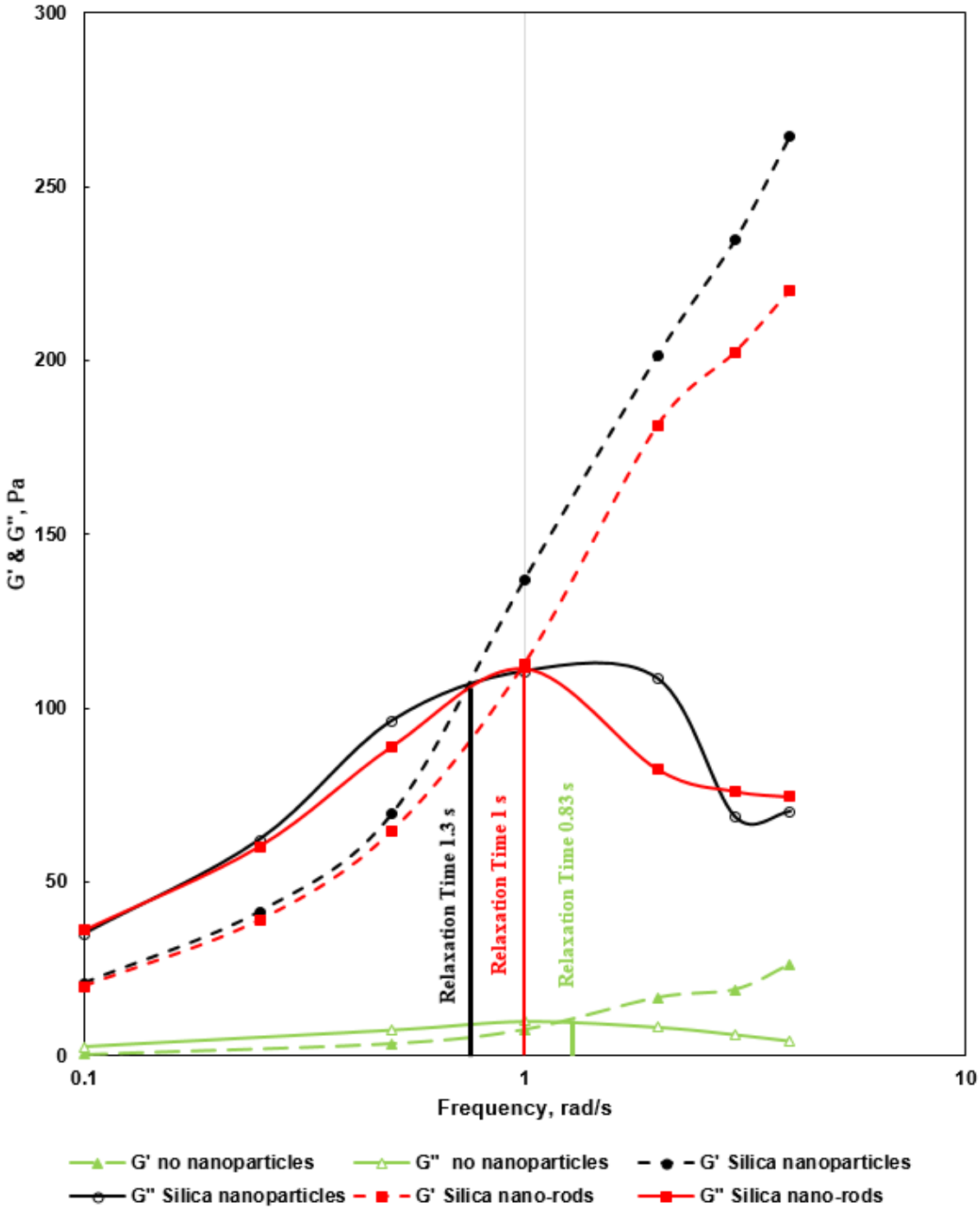

Fig. 22- DOM of fracturing fluid with and without the different types of silica nanoparticles (rods and spheres). The tests were conducted at 50% strain and at 280°F.

The magnitude of the relaxation time is highly correlated to dominance of elastic behavior over viscous behavior, which in turn means the higher the relaxation time, the more elastic the fluid behaves. The dominance of elastic behavior over viscous behavior magnifies higher crosslinking and micelle-micelle entanglement (Knoll and Prud'homme 1987; Loveless et al. 2011, Malhotra and Sharma 2011). These outcomes indicate that both types of silica nanoparticles are able to achieve pseudo-crosslinking of the VES micelles and make it a more elastic dominant fluid with higher relaxation time. Examining the storage modulus profile at low frequency, it can be concluded that it is dependent on frequency. This dependency shows that the crosslinking nature is not ideal in all 3 dimensions which attributes to pseudo-crosslinking (Knoll and Prud'homme 1987).

DOM was also carried out on both types of iron oxide nanoparticles. The data presented in Fig. 23 displays a similar enhancement the iron oxide nanoparticles has on the storage and loss moduli of the VES system compared to the effect of the silica nanoparticles. In this case, the iron oxide nanoparticles actually has a more positive impact on the fluid relaxation time increasing it up to 1.6s, thus increasing the degree of micelle-micelle entanglement and pseudo-crosslinking than the silica nanoparticle enhanced fracturing fluids.

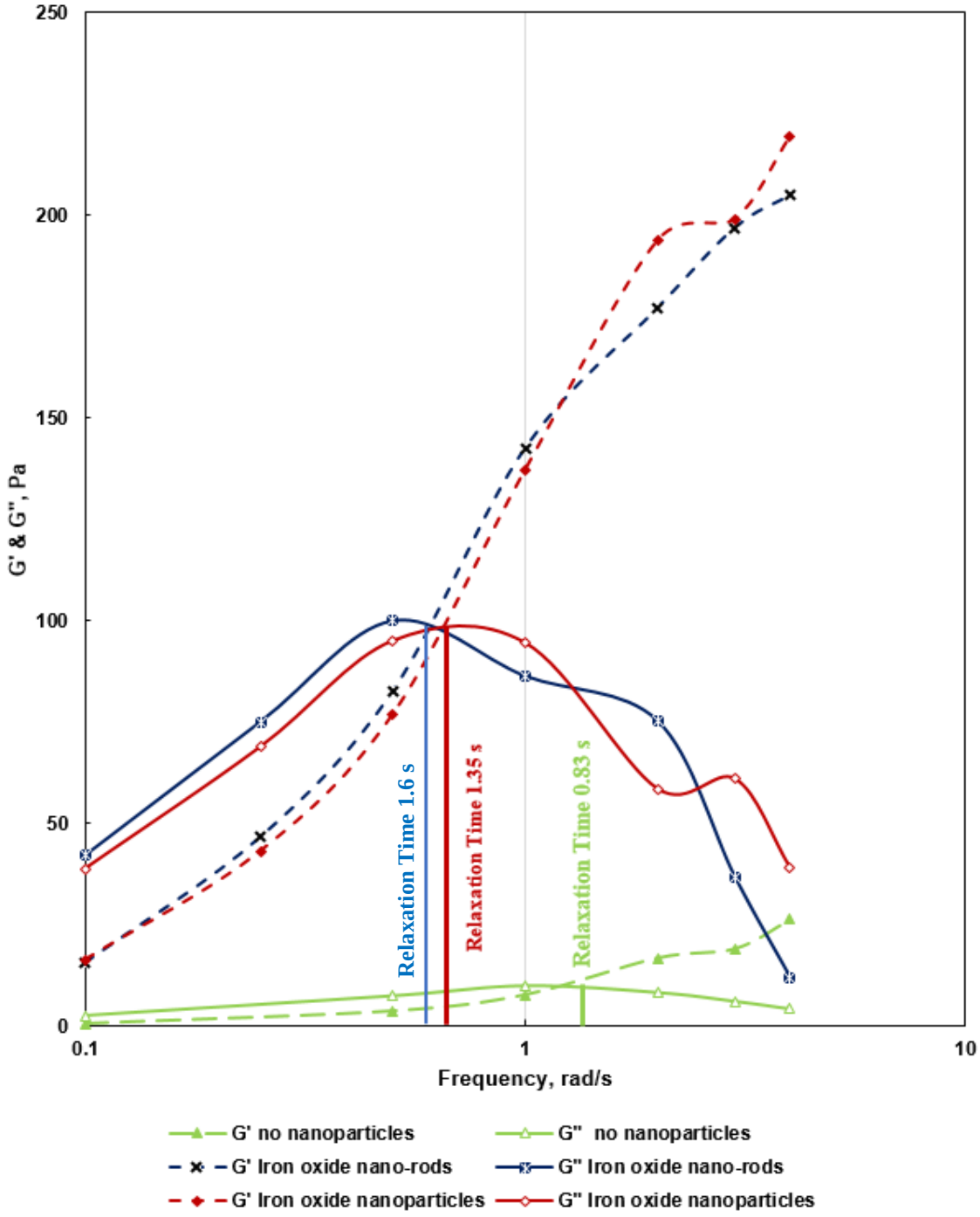

Fig. 23- DOM of fracturing fluid with and without the different types of iron nanoparticles (rods and octahedral). The tests were conducted at 50% strain and at 280°F.

Table 7- Relaxation times of Fracturing fluids at 50% Strain and 280°F

Solution	Relaxation Time (s)
VES	0.83
VES + Silica nanorods	1
VES + Silcia nanospheres	1.3
VES + Iron Oxide nanorods	1.6
VES + Iron oxide octahedral nanoparticles	1.35

3.11 Proppant Settling Test

When comparing the measurement of the VES fluid proppant carrying capacity between the fracturing fluid containing silica nanospheres and the fracturing fluid carrying none, the fluid containing silica nanospheres outperforms the other significantly. Fig. 24 displays images taken during a four hour period at 280°F and the fluid containing silica nanospheres was able to retain full proppant suspension for 60 min. After 80 min, the top 20 ml of the fracturing fluid experienced a decrease in the concentration of the proppant. After 240 min, the top 30 ml did not contain any proppants. Comparing this fluid to the fracturing fluid containing no silica nanospheres, the performance was a lot less.

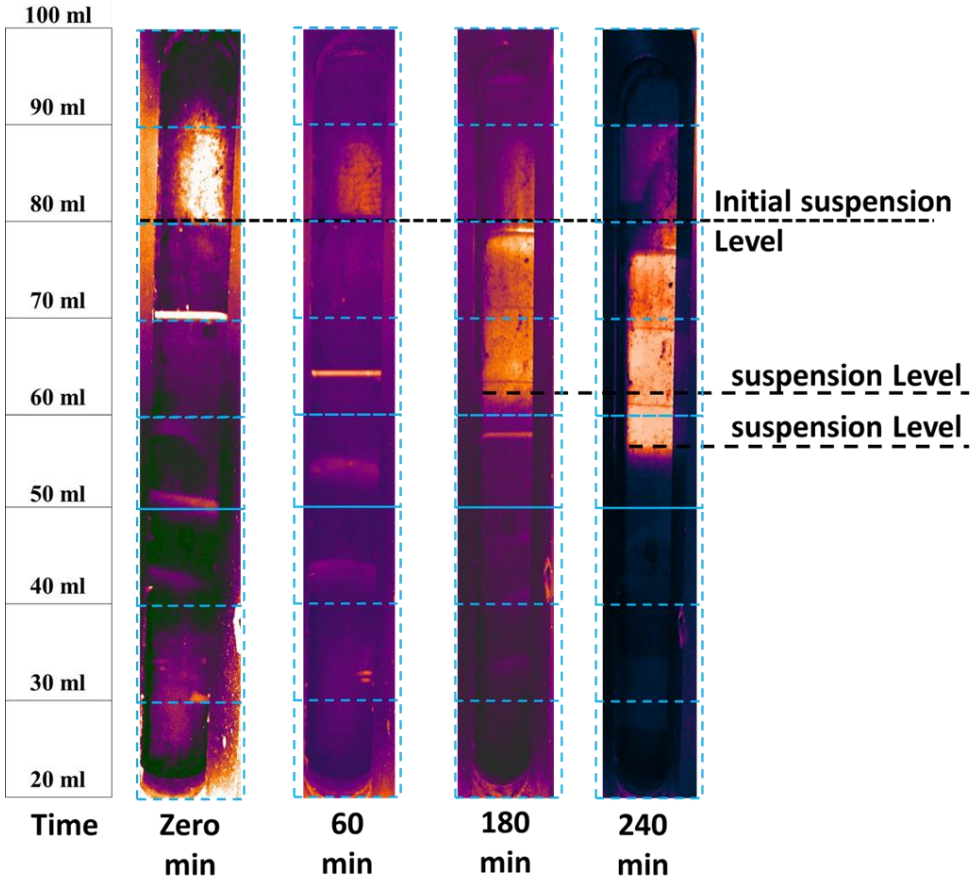

Fig. 24- Sand proppant 20/40 settling in 4 wt% VES based fracturing fluid containing 7 pptg silica nanospheres and 23 wt% $CaCl_2$ at 280ºF.

Fig. 25 displays the quick settling of the proppants within the first 60 min of the test. The top 20 ml of the fluid witnessed a decrease in proppant concentration which continued until 240 min, where a proppant free solution was yielded. This data showed that the presence of silica nanoparticles lead to a 100 time boost in storage moduli and boost in relaxation time which led to enhanced VES micelle entanglement, pseudo crosslinking state, and proppant carrying capacity.

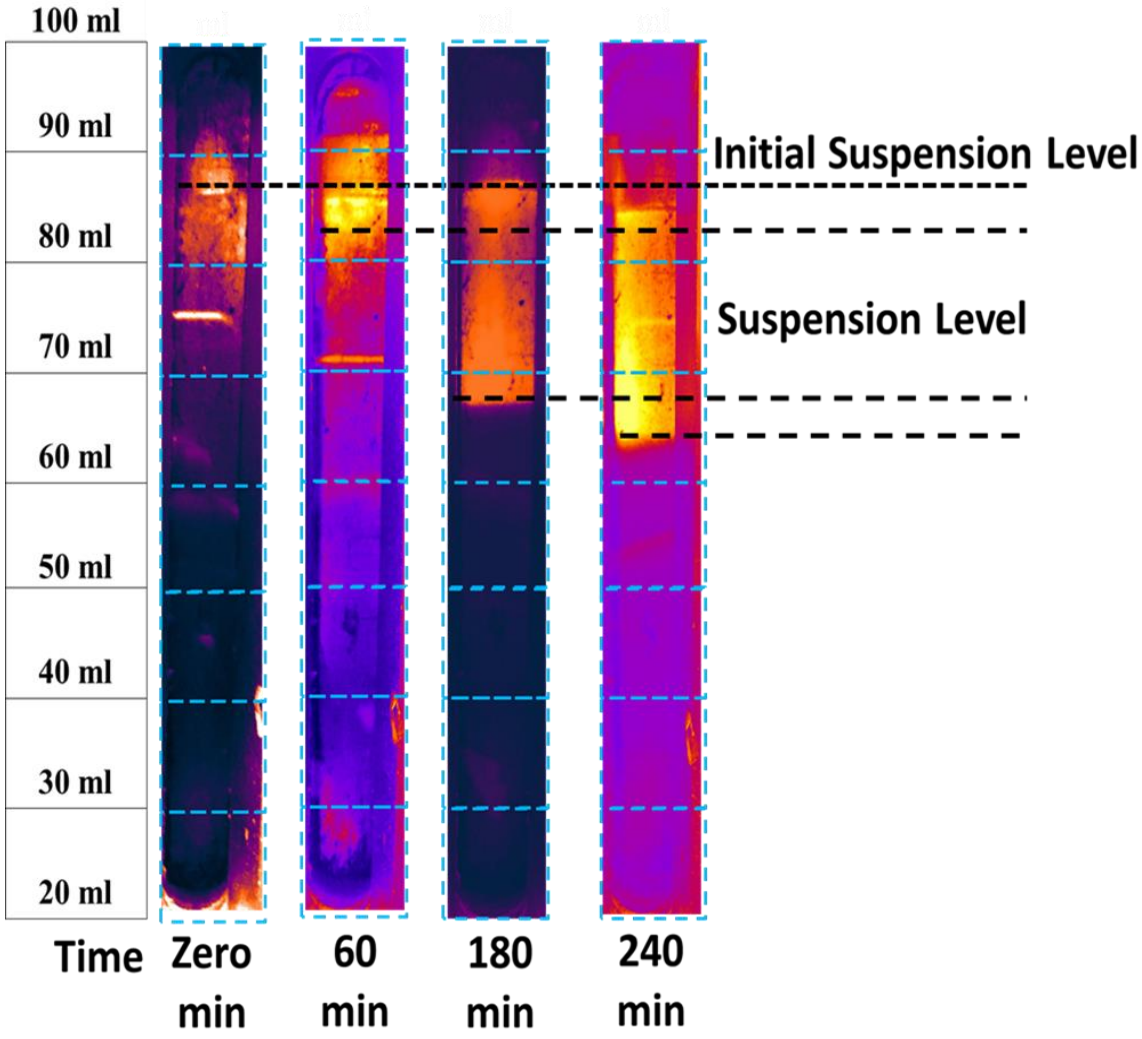

Fig. 25- Sand proppant 20/40 settling in 4 wt% VES based fracturing fluid containing no nanoparticles and 23 wt% $CaCl_2$ at 280°F.

3.12 Filter Loss and Formation Damage Characteristics

The fracturing fluid containing no nanoparticles and the silica nanospheres were pumped across the core with a differential pressure of 400 psi and at a temperature of 280^{o}F. The filtration rate is represented in Fig. 26 and a deep analysis can be drawn from the data. The fracturing fluid containing the silica nanospheres displayed a quick decrease in flow rate within 1 minute, from 80 cm^3/min to 3 cm^3/min. After this decline, the flow rate continued to decrease to 1 cm^3/min. The fracturing fluid containing no silica nanospheres displayed the same behavior in flow rate, however the time frame this happened in was 16 min. These events are evidence that the fluid containing no nanoparticles is inadequate to form an efficient filter cake that invades the core and cause penetrating formation damage. The volume of fracturing fluid pumped through the core that contains no nanoparticles is about twice the volume of that of the fluid containing silica nanospheres. The data shows that with the presence of silica nanospheres, the fracturing fluid can form a filter cake that limits VES leakage into the formation. The addition of silica nanospheres has a positive impact on the fluid loss rate, fluid invasion in the formation, and VES breakability.

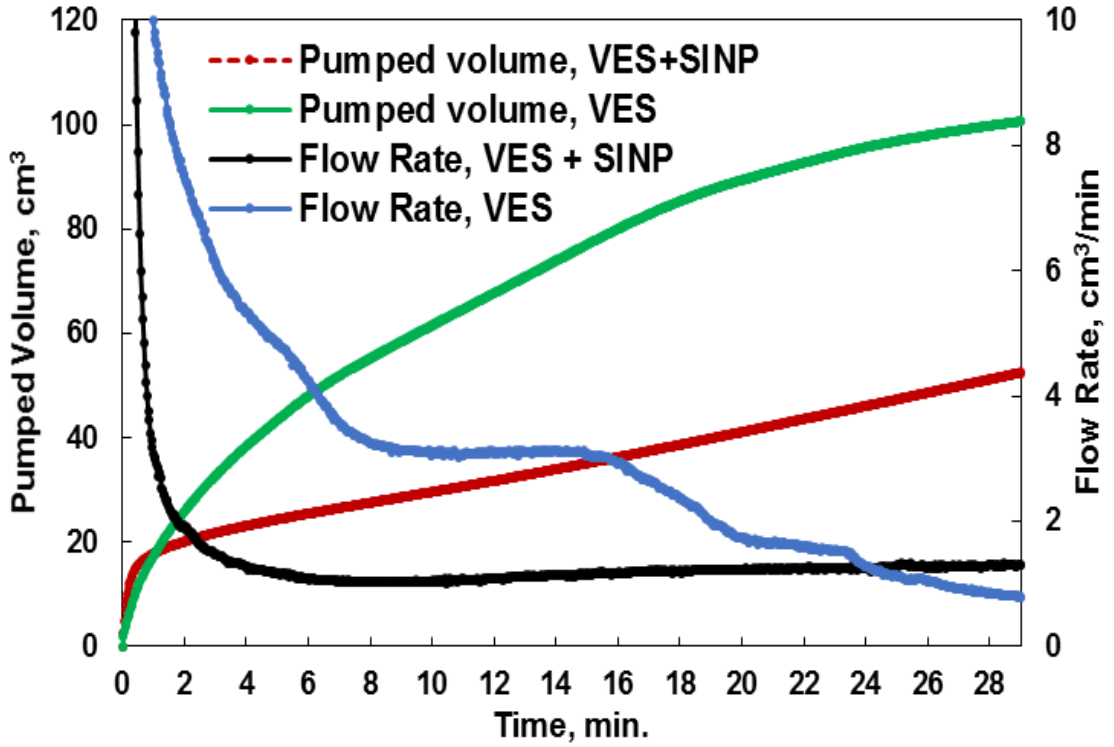

Fig. 26- Filter loss rate and pumped volume of fracturing fluid containing no and silica nanospheres in 30 min time period at differential pressure of 400 psi and 280ºF.

The permeability of the cores before and after exposure of the fracturing fluids are displayed in Table 3. For the core exposed to the fluid with no silica nanospheres, the initial permeability was 65 md, and for the core that was exposed to fluid containing the silica nanospheres, the permeability was 54 md. After being exposed to the fracturing fluids, the permeability of both the cores decreased to 10 md and 21 md respectively. The filter loss rate of the fluid containing no silica nanospheres was 75 cm^3/ 30min, while the filter loss rate of the fluid containing the nanoparticles was 30 cm^3/ 30min. This outcome indicates that the fluid containing the silica nanospheres has a much higher advantage than

the fluid containing no nanoparticles in terms of forming a quick filter cake, filtration rate, and depth of core damage.

Table 8- Filter loss rate, Formation damage, VES fluid breakability in Buff Barea sandstone at differential pressure of 400 psi at 280ºF

Core Properties	VES at 280ºF	VES + silica nanospheres at 280ºF
$K_{initial}$, md	56	64
$K_{damaged}$, md	10	21
K_{Clean}, Mutual Solvent 12 hours, md	50	54
Filter loss, cm^3/30min	75	30

Compute tomography (CT) was utilized to calculate the extent of fracturing fluid invasion of the core. The fracturing fluid breakability was also assessed using this method. From Fig. 27, it is evident that the core being pumped with fracturing fluid containing no nanoparticles experiences severe invasion from the inlet to the outlet. Pumping mutual solvent and maintaining it overnight removes 90% of the fracturing fluid initially present. Fig. 28 displays the outcome of the core that was treated with the fracturing fluid containing the silica nanospheres. The figure displays a partial invasion of fluid into the core that is approximately halfway through. After overnight soaking of the core with mutual solvent, 90% of it is removed. In both cases, most of both fracturing fluids was recovered.

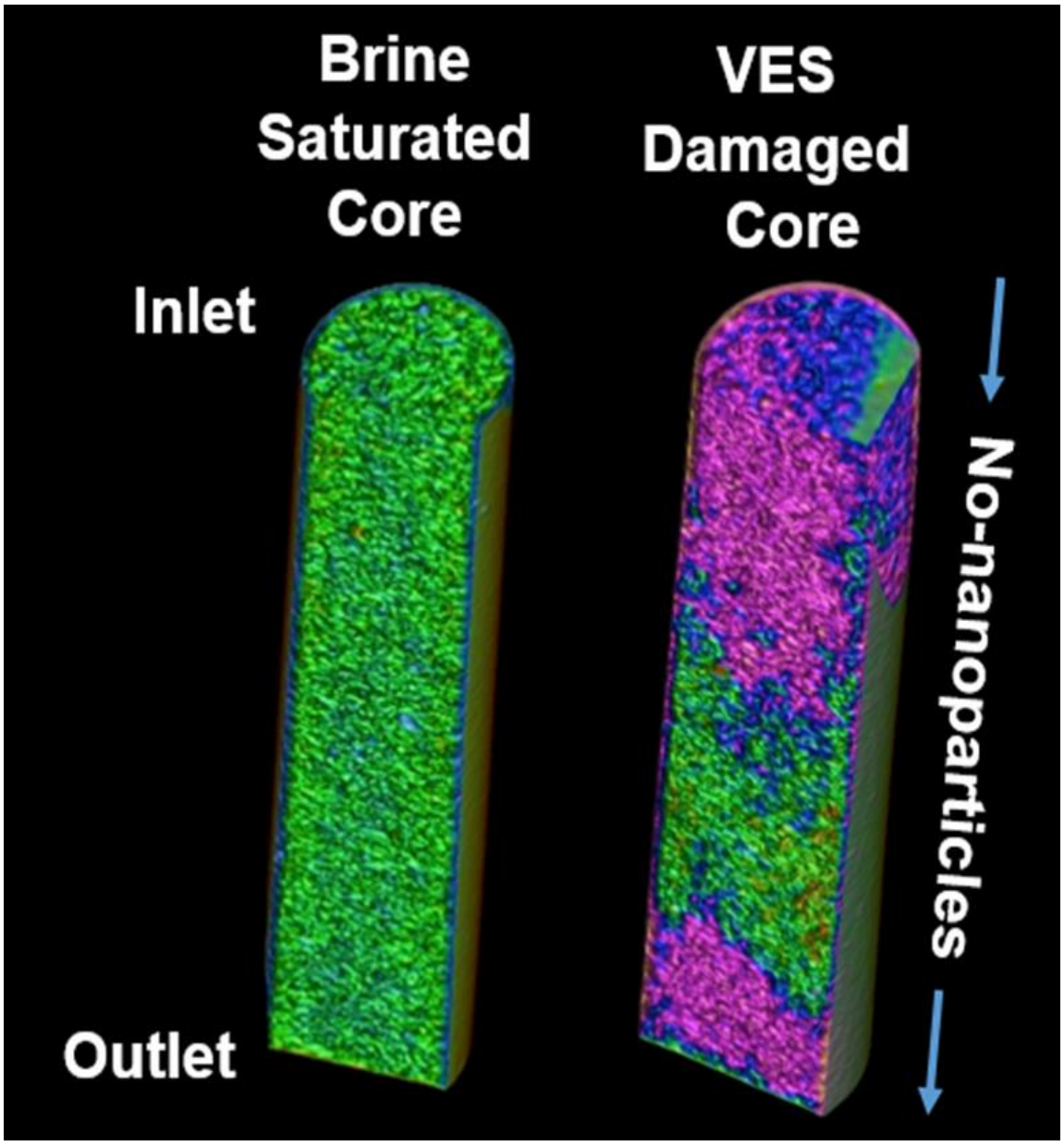

Fig. 27- CT analysis of Buff Berea sandstone before and after VES fluid invasion at 280°F. The core was treated with 5 wt% NH_4Cl brine, fracturing fluid containing 4 wt% VES and 23 wt% $CaCl_2$, and 5 wt% NH_4Cl brine. Purple: severe damage, Blue: moderate damage, Green: no blockage.

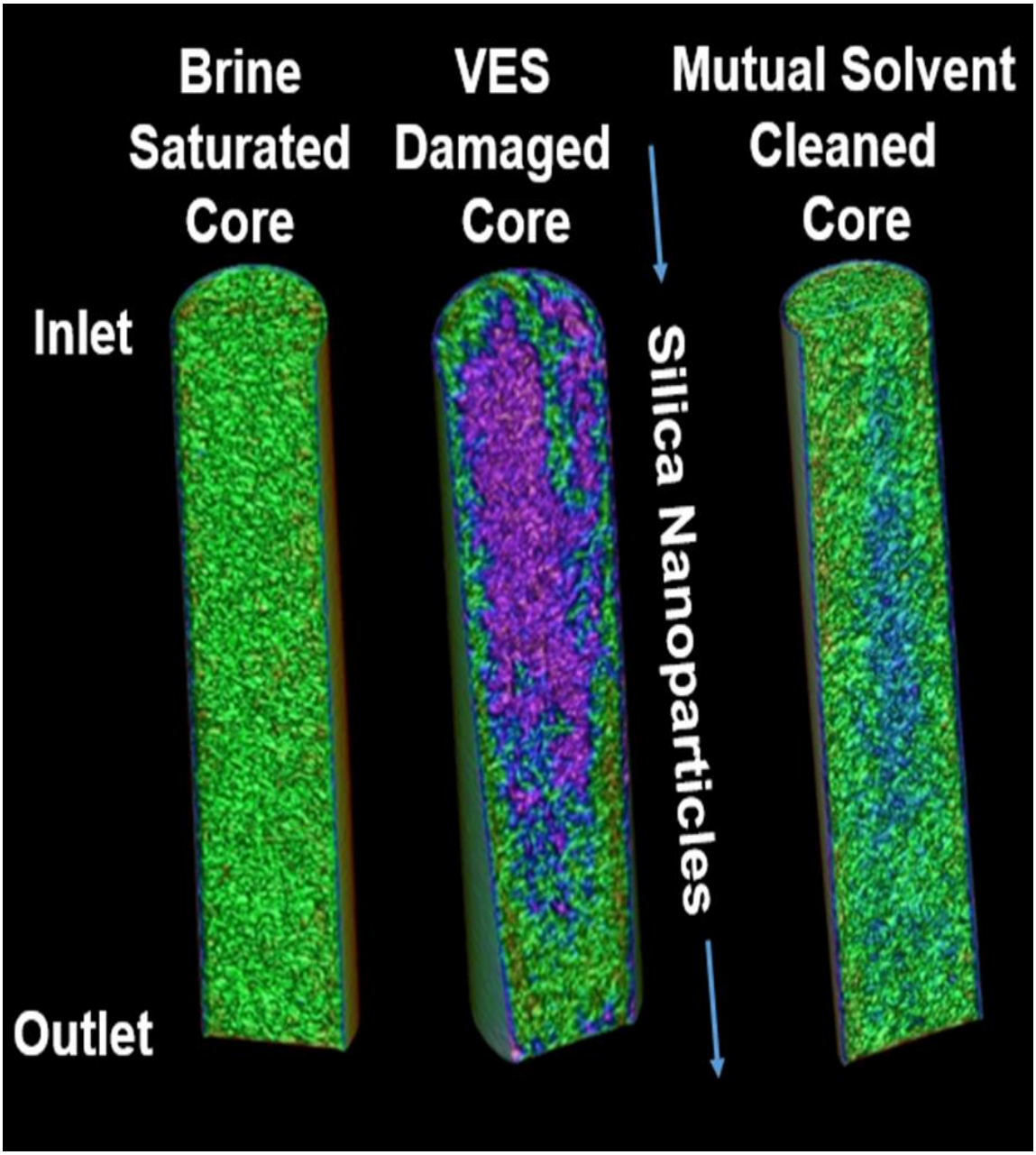

Fig. 28- CT analysis of Buff Berea sandstone before and after VES fluid invasion at 280°F. The core was treated with 5 wt% NH_4Cl brine, fracturing fluid containing 4 wt% VES and 23 wt% $CaCl_2$ and 7 pptg silica nanorods, and 5 wt% NH_4Cl brine. Purple: severe damage, Blue: moderate damage, Green: no blockage.

CHAPTER IV

CONCLUSION

This work investigated the influence of different types of nanoparticles, their shape, their size, and their surface properties on the viscosity enhancement of zwitterionic VES. In detail, the micellization and crosslinking process was analyzed at varying concentrations of VES ranging from 2 and 4 wt% in 23 wt% $CaCl_2$ brine. Thermal sensitivity of the zwitterionic VES was analyzed under the influence of the different types of nanoparticles in question, and based off the results, the following conclusions can be made:

1. The addition of silica nanoparticles, both spherical and rod-shaped, to a 4 wt% VES system that contains 23 wt% $CaCl_2$ contributes to a 50% enhancement of the apparent viscosity at 280^{o}F.
2. The spherical and octahedral nanoparticles of both silica and iron oxide have a negative impact on the apparent viscosity of the 4 wt% VES system at 280^{o}F.
3. At higher temperatures, specifically 350^{o}F, the addition of spherical silica nanoparticles and octahedral iron oxide nanoparticles increases the apparent viscosity of the base fluid by 9 times.
4. When decreasing the concentration of the VES to 2 wt% VES at 280^{o}F, both the silica and iron oxide nanorods have a positive impact on the apparent viscosity, increasing it to 25% of the original value initially. However, the silica nanorods are the only nanoparticles that stabilize the system for 1 hour.

5. With a system of 2 wt% VES, both the silica nanospheres and the iron oxide octahedral nanoparticles have a negative impact on the VES system. A reduction of 90% of the apparent viscosity was observed.
6. Adding nanoparticles to the VES system, specifically silica nanospheres and iron oxide nanorods, results in robust crosslinking of the micelles and increase the proppant carrying capacity of the fracturing fluid.
7. Adding silica nanospheres to the fracturing fluid reduces the filtration rate significantly, fluid invasion of the formation, and eases the VES breakability via mutual solvent.

REFERENCES

Al-Muntasheri, G. A., Liang, F., and Hull, K. L. 2017. Nanoparticle-Enhanced Hydraulic-Fracturing Fluids: A Review. SPE Prod & Oper 32 (2): 186-195. SPE-185161-PA. https://doi.org/10.2118/185161-PA.

Cates, M.E. 1990. Nonlinear viscoelasticity of wormlike micelles (and other reversibly breakable polymers). *The Journal of Physical Chemistry* **94** (1): 371—375. http://dx.doi.org/10.1021/j100364a063.

Chase, B., Chmilowski, W., and Dang, Y. 1997. Clear fracturing fluids for increase well productivity. *Oilfield Review* **20**, 33.

Crews, J. B. and Gomaa, A. M. 2012. Nanoparticle Associated Surfactant Micellar Fluids: An Alternative to Crosslinked Polymer Systems. Presented at the SPE International Oilfield Nanotechnology Conference and Exhibition, Noordwijk, The Netherlands, 12-14 June. SPE-157055-MS. https://doi.org/10.2118/157055-MS.

de Vries, W., Doerenkamp, C., Zeng, Z. et al. 2016. Synthesis and characterization of amorphous mesoporous silica using TEMPO-functionalized amphiphilic templates. Journal of Solid State Chemistry 237 (1): 93-98.

Drye, T. J. and Cates, M. E. 1992. Living Networks: The Role of Cross-Links in Entangled Surfactant Solutions. Chemical Physics 96 (2): 1,367-1,375.

Fakoya, M. F. and Shah, S. N. 2013. Rheological Properties of Surfactant-Based and Polymeric Nano-Fluids. Presented at the SPE/ICoTA Coiled Tubing & Well Intervention Conference & Exhibition, The Woodlands, Texas, 26-27 March. SPE-163921-MS. https://doi.org/10.2118/163921-MS.

Feng Y., Chu Z., and Dreiss C.A. 2015. Thermo-responsive Wormlike Micelles. In: Smart Wormlike Micelles. SpringerBriefs in Molecular Science. Springer, Berlin, Heidelberg.

Farge, E. and Maggs, A.C. 1993. Dynamic scattering from Semiflexible Polymers. *ACS Publications* **26** (19): 5041—5044. http://dx.doi.org/10.1021/ma00071a009.

Gomaa, A. M., Gupta, D. V. S., and Carman, P. 2015. Viscoelastic Behavior and Proppant Transport Properties of a New High-Temperature Viscoelastic Surfactant-Based Fracturing Fluid. Presented at the SPE International Symposium on Oilfield Chemistry, The Woodlands, Texas, 13-15 April. SPE-173745-MS. https://doi.org/10.2118/173745-MS.

Goodwin, J. W. 2009. Colloids and Interface with Surfactants and Polymers. West Sussex, UK: Wiley and Sons Ltd.

Gurluk, M. R., Nasr-El-Din, H. A., and Crews, J. B. 2013. Enhancing the Performance of Viscoelastic Surfactant Fluids Using Nanoparticles. Presented at the EAGE Annual Conference & Exhibition incorporating SPE Europec, London, UK, 10-13 June. SPE-164900-MS. https://doi.org/10.2118/164900-MS.

Gurluk, M.R., Wang , G., Nasr-El_din, H.A. et al. 2013. The Effect of Different Brine Solutions on the Viscosity of VES Micelles. *Journal of Petroleum Technology*. SPE-165164-MS. http://dx.doi.org/10.2118/165164-MS.

Hanafy , A., Najem, F., and Nasr-El-Din, H.A. 2018. Impact of Nanoparticles Shape on the VES Performance for High Temperature Applications. *Journal of Petroleum Technology*. SPE-190099. http://dx.doi.org/10.2118/190099.

Hanafy, A. M., Nasr, M. I., El-Sheltawy, S. T. et al. 2014. Preparation of Nano-Magnetite Whiskers, Rods, and Needles Using Ultrasonic Bathing with Co-Precipitation Technique. Presented at The International Conference of Solid Waste Technology and Management, Philadelphia, 30 March to 2 April.

Helgeson, M. E., Hodgdon, T. K., Kaler, E. W., et al. 2010. Formation and Rheology of Viscoelastic "Double Networks" in Wormlike Micelle-Nanoparticle Mixtures. Langmuir 26 (11): 8,049-8,060.

Huang, T. and Crews, J. B. 2008. Nanotechnology Applications in Viscoelastic Surfactant Stimulation Fluids. SPE Prod & Oper 23 (4): 512-517. SPE-107728-PA. https://doi.org/10.2118/107728-PA.

Huang, T., Crews, J. B., and Agrawal, G. 2010. Nanoparticle Pseudocrosslinked Micellar Fluids: Optimal Solution for Fluid-Loss Control with Internal Breaking. Presented at the SPE International Symposium and Exhibition on Formation Damage Control, Lafayette, Louisiana, 10-12 February. SPE-128067-MS. https://doi.org/10.2118/128067-MS.

Klein, R. 2002. Interacting Colloidal Suspensions. *Neutrons, X-rays and Light: Scattering Methods Applied to Soft Condensed Matter*, 1st ed.:351-380
Kline, S.R. and Kaler, E.W. 1996. Interactions in binary mixtures: Partial structure factors in mixtures of sodium dodecyl sulfate micelles and colloidal silica. *The Journal of Chemical Physics* **105** (9): 3813—3822. http://dx.doi.org/10.1063/1.472202.

Knoll, S. K. and Prud'homme, R. K. 1987. Interpretation of Dynamic Oscillatory Measurements for Characterization of Well Completion Fluids. Presented at the SPE International Symposium on Oilfield Chemistry, San Antonio, Texas, 4-6 February.

SPE-16283-MS. https://doi.org/10.2118/16283-MS.

Langford, J. I. and Wilson, A. J. C. 1978. Scherrer after sixty years: a survey and some new results in the determination of crystallite size. Journal of Applied Crystallography, 11 (2): 102-113.

Li, L., Ozden, S., Al-Muntasheri, G.A. et al. 2018. Nanomaterials-Enhanced Hydrocarbon-Based Well Treatment Fluids. *Journal of Petroleum Technology*. SPE-189960. http://dx.doi.org/10.2118/189960.

Loveless, D., Holtsclaw, J., Saini, R. et al. 2011. Fracturing Fluid Comprised of Components Sourced Solely from the Food Industry Provides Superior Proppant Transport. Presented at the SPE Annual Technical Conference and Exhibition, Denver, Colorado, 30 October-2 November. https://doi.org/10.2118/147206-MS.

Malhotra, S. and Sharma, M. M. 2011. A General Correlation for Proppant Settling in VES Fluids. Presented at the SPE Hydraulic Fracturing Technology Conference, The Woodlands, Texas, 24-26 January. SPE-139581-MS. https://doi.org/10.2118/139581-MS.

Nemoto, N., Kuwahara, M., Yao, M.L. et al. 1995. Dynamic Light Scattering of CTAB/NaSal Threadlike Micelles in a Semidilute Regime. 3. Dynamic Coupling between Concentration Fluctuation and Stress. *Langmuir* **11** (1): 30—36. http://dx.doi.org/10.1021/la00001a009.

Nettesheim, F. and Wagner, N.J. 2007. Fast Dynamics of Wormlike Micellar Solutions. *Langmuir* **23** (10): 5267—5269. http://dx.doi.org/10.1021/la0635855.

Nettesheim, F., Liberatore, M. W., Hodgdon, T. K., et al. 2008. Influence of Nanoparticle Addition on the Properties of Wormlike Micellar Solutions. Langmuir 24 (15): 7,718-7,726.

Ozden, S., Li, L., Al-Muntasheri, G.S. et al. 2017. Nanomaterials-Enhanced High-Temperature Viscoelastic Surfactant VES Well Treatment Fluids. *Journal of Petroleum Technology*. SPE-184551. http://dx.doi.org/10.2118/184551-MS.

Pedersen, J.S. and Schurtenberger, P. 1996. Scattering Functions of Semiflexible Polymers with and without Excluded Volume Effects. *Macromolecules* **29** (23): 7602—7612. http://dx.doi.org/10.1021/ma9607630.

Pletneva, V. A., Molchanov, V. S., and Philippova, O. E. 2015. Viscoelasticity of Smart Fluids Based on Wormlike Surfactant Micelles and Oppositely Charged Magnetic Particles. Langmuir 31 (1): 110-119.

Rahmani, S., Durand, J. O., Charnay, C. et al. 2017. Synthesis of Mesoporous Silica Nanoparticles and Nanorods: Application to Doxorubicin Delivery. Solid State Sciences 68 (1): 25-31.

Rehage, H. and Hoffmann, H. 1991. Viscoelastic Surfactant Solutions: Model Systems for Rheological Research. Molecular Physics 74 (5): 933-973.

Samuel, M., Polson, D., Graham, D. et al. 2000. Viscoelastic Surfactant Fracturing Fluids: Applications in Low Permeability Reservoirs. Presented at the SPE Rocky Mountain Regional/Low-Permeability Reservoirs Symposium and Exhibition, Denver, Colorado, 12-15 March. SPE-60322-MS. https://doi.org/10.2118/60322-MS.

Sangaru, S. S., Yadav, P., Huang, T. et al. 2016. Temperature Dependent Influence of Nanoparticles on Rheological Properties of VES Fracturing Fluid. Presented at the SPE/IATMI Asia Pacific Oil & Gas Conference and Exhibition, Jakarta, Indonesia, 17-19 October. SPE-186308-MS. https://doi.org/10.2118/186308-MS

Sangaru, S. S., Yadav, P., Huang, T. et al. 2017. Improved Fluid Efficiency for High-Temperature Viscoelastic Surfactant Based Stimulation Fluids Using Synergistic Effects of Nanoparticles. Presented at the SPE Kingdom of Saudi Arabia Annual Technical Symposium and Exhibition, Dammam, Saudi Arabia, 25-28 April. SPE-182807-MS. https://doi.org/10.2118/182807-MS

Spenley, N.A., Cates, M.E., and McLeish, T.C.B. 1993. Nonlinear rheology of wormlike micelles. http://dx.doi.org/10.1103/PhysRevLett.71.939.

Shikata, T., Dahman, S.J., and Pearson, D.S. 1994. Rheo-Optical Behavior of Wormlike Micelles. *Langmuir* **10** (10): 3470—3476. http://dx.doi.org/10.1021/la00022a019.

Von Berlepsch, H., Harnau, L., and Reineker, P. 1998. Persistence Length of Wormlike Micelles from Dynamic Light Scattering. *The Journal of Physical Chemistry B* **102** (39): 7518—7522. http://dx.doi.org/10.1021/jp980677x.

Willenbacher, N., Oelschlaeger, C., Schopferer, M. et al. 2007. Broad Bandwidth Optical and Mechanical Rheometry of Wormlike Micelle Solutions. *Physical Review Letters* **99** (6). http://dx.doi.org/10.1103/PhysRevLett.99.068302.

Willenbacher, N. and Oelschlaeger, C. 2007. Dynamics and structure of complex fluids from high frequency mechanical and optical rheometry. *Elsevier* **12** (1): 43—49. http://dx.doi.org/10.1016/j.cocis.2007.03.004.

Yang, J. 2002. Viscoelastic wormlike micelles and their applications. *Current Opinion in Colloidal and Interface Science* **7**: 276—281.

Yu, M., Mu, Y., Wang, G. et al. 2012. Impact of Hydrolysis at High Temperatures on the Apparent Viscosity of Carboxybetaine Viscoelastic Surfactant-Based Acid: Experimental and Molecular Dynamics Simulation Studies. SPE J. 17 (4): 1,119-1,130. SPE-142264-PA. https://doi.org/10.2118/142264-PA.

Zhang, Y. and Cremer, P. S. 2006. Interactions Between Macromolecules and Ions: The Hofmeister Series. Current Opinion in Chemical Biology 10 (6): 658-663.

Zhang, Y., An, P., and Liu, X. 2015. A "worm"-containing viscoelastic fluid based on a single amine oxide surfactant with an unsaturated C22-tail. *RSC Advances* **5** (25), 19135-19144. http://dx.doi.org/10.1039/C4RA16772D.

Zilman, A.G. and Granek, R. 1996. Undulations and Dynamic Structure Factor of Membranes. *Physical Review Letters* **77**(23): 4788-4791. http://dx.doi.org/10.1103/PhysRevLett.77.4788.